Master's Thesis

Master's Degree in Nuclear Engineering

Safety-informed design of lead-cooled reactors on mobile platforms

Guillem Sanchis Ramírez

April 2022

Director: Lluís Batet Miracle

Supervisor: Janne Wallenius

Call: April 2022

Escola Tècnica Superior
d'Enginyeria Industrial de Barcelona

Abstract

Nuclear power has a prominent role to play in the energy landscape of the 21st century. Together with large reactor designs that make the most out of economies of scale, small, modular reactors (SMR) may also play a role thanks to their potential modular, factory-based and fast deployment, which have the potential to minimize the capital cost of nuclear, which is one of its main drawbacks. Among such designs, lead-cooled fast reactors (LFR) present some unique strengths, among others their lack of pressurization of the primary system and their potential to passively remove decay heat by means of natural convection. The SUNRISE project, in Sweden, is an effort by, among others, KTH to prove the feasability of this technology.

In that context, the analytical design tool *ADELE*, which draws from the BELLA code produced at KTH, is developed. Its goal is to provide a fast-to-iterate algorithm that uses basic physics constraints to obtain the core design without relying on more computationally costly methods, like Monte Carlo simulations, which are regularly used for that purpose. Specifically, a system that is capable of removing all the residual heat via convective cooling is obtained from a short list of basic input values. This algorithm is implemented into a mobile application, with the goal of being available to Nuclear Engineering students. The resulting code is capable of replicating reference core designs with a reasonable degree of accuracy, given the simplicity of the assumptions used in the process.

Contents

List of Figures

1 Introduction

There is not the slightest indication that nuclear energy will ever be obtainable.
It would mean that the atom would have to be shattered at will.
— Albert Einstein (1932)

1.1 Background and prospects of nuclear power

Throughout the course of history, the progress of mankind has been inextricably tied to its consumption of energy resources in general, and access to reliable electricity in particular; a trend that continues to this day[1].

Since its debut in the 1950s and subsequent global deployment in the following two decades, the commercial generation of electrical power by means of nuclear fission remains the safest, cleanest[2] and cheapest[3] baseload generation available, remaining the only one that is both low-carbon and deployable at large scale anywhere on the world[1].

However, the mixed early history of the technology, with its conception closely tied to nuclear weapons development; together with rising costs[4] and the increased public perception of its danger following the Three Mile Island and, to a larger extent, Chernobyl accidents, largely put a stop on the rapid deployment growth that nuclear power had enjoyed around most of the world[5].

In the last two decades, the effects of the Fukushima Daiichi accident on public perception notwithstanding, there has been a timid trend towards the reconsideration of nuclear power technology as a relevant sector of the energy mix[6, 7, 8, 9]. This sometimes-called *Nuclear Renaissance* has been driven by the prospect of rising fossil fuel prices, together with the pressure from anthropogenic global warming to *i*) electrify polluting sectors such as land transportation and heavy industries like steel and cement, while *ii*) shifting towards a low-emissions electricity grid. Indeed, the World Energy Council concluded that nuclear power has the potential to contribute to 10 out of the 17 Sustainable Development Goals (SDG) set by the UN in 2015[10].

[1] The term *baseload* refers to the constant minimum amount of power demand in a grid, as opposed to *peaking* generation, which is deployed intermittently to respond to daily or seasonal oscillations. Both hydroelectric and geothermal power are renewable and constant, but their application is limited to those regions with suitable geology and geography.

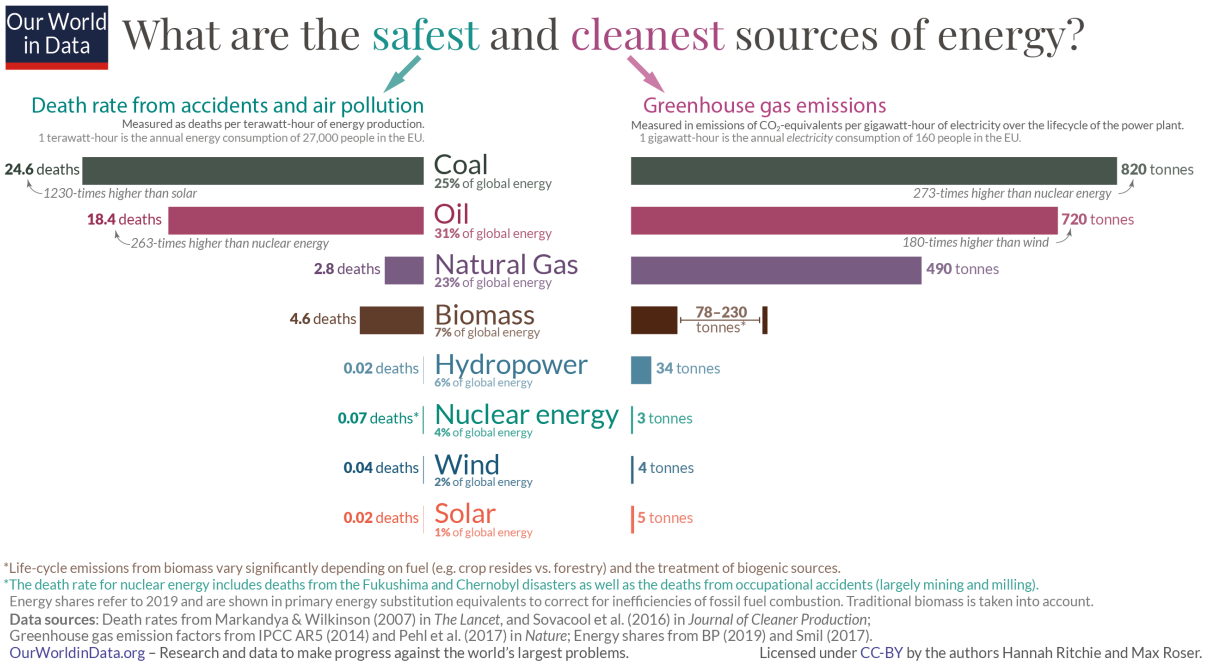

Figure 1.1: Death rates and greenhouse emissions per unit of energy produced of various power technologies. Death rates include both air pollution effects and accidents. Source:[2], licensed under CC BY.

1.1.1 Economics of nuclear power. Small modular reactors (SMR)

Unlike fossil-fuelled baseload power plants, i.e. gas and coal facilities, the cost of operation, and the cost of the fuel itself, are not a large component of the overall cost when considering nuclear power[11]. This makes them attractive in the face of potential fuel cost inflation. Instead, given their increased complexity and therefore lead times, the construction cost is a proportionally larger component, upwards of 60% overall[12]. This includes both the cost of construction itself, sometimes dubbed *overnight* cost, as well as the cost of financing incurred between the start of the construction and the commissioning of the plant. The latter is usually larger compared to, say, a gas-fired power plant of equal magnitude, reflecting a perception that the increased complexity implies an increased risk in the investment.

Given the above, then, shortening construction times of new nuclear power plants, together with reducing the variance in expected costs, is crucial for the technology to be a viable option for base generation. This explains the interest by the IAEA to promote the commercialization of small modular reactors (SMRs)[13], typically defined as having an electical power output up to 300 MW. There are currently about 50 such designs, with technology ranging from scaled down evolutions of current designs to Generation IV systems. They have a series of advantages when compared to conventional nuclear reactors:

- Their smaller scale, together with their potential to be serially built, give them the prospect of having much shorter construction times, and therefore of carrying a significantly lower cost.

- Their modular nature allows for flexible deployment, allowing for the capacity to gradually replace fossil-fuelled facilities, as well as permitting grids to adapt over time to changing

conditions, in particular the gradual penetration of variable renewable sources. Furthermore, this also allows for the possibility of locating them closer to the point of consumption, opening up the options for additional features such as cogeneration, as well as for their deployment to remote areas.

- Their lower power density translates to their ability to be passively safe.

On the other hand, reducing the power density of nuclear reactor negates the gains from economies of scale, which have consistently driven commercial reactor designs; from the tens of thermal megawatts of the first power plants to current facilities, with well over a gigawatt of thermal power per reactor. Instead, the modular approach may lead to proportionally larger operational expenses, given the increased number of units. Whether this increase in specific cost can be offset by savings from modular construction in factory environments and other purported cost savings in SMRs remains an open discussion.

1.1.2 Generation IV technology

The Generation IV International Forum (GIF) was established in 2001 by the US Department of Energy's Office of Nuclear Energy together with representatives of Argentina, Brazil, Canada, France, Japan, the Republic of Korea, the Republic of South Africa, and the United Kingdom, with the goal of "[developing] the research necessary to test the feasibility and performance of fourth generation nuclear systems")[14]. In this framework, Generation IV reactor technologies would "use fuel more efficiently, reduce waste production, be economically competitive, and meet stringent standards of safety and proliferation resistance", compared to conventional designs.

The GIF considers 6 reactor designs to be the most promising to address its stated goals[15]. They are:

- Gas-cooled Fast Reactors (GFR)
- Lead-cooled Fast Reactor (LFR)
- Molten Salt Reactor (MSR)
- Supercritical Water-cooled Reactor (SCWR)
- Sodium-cooled Fast Reactor (SFR)
- Very High Temperature Reactor (VHTR)

As [16] points out, while all six of the above technologies were implemented at the prototype stage in the early days of nuclear research, they were eventually incapable of competing commercially with PWR and BWR designs. Of those, only SFRs were deployed at industrial scale at all, with the most notable cases being the French Phénix and SuperPhénix prototypes, in Creys-Malville, and the Russian BN-600 and BN-800 in Beloyarsk, the latter two currently in operation. Lead-bismuth reactors were used in Soviet and Russian military submarines, while helium-cooled high temperature designs (750-950°C) have mostly remained prototypes and research reactors. As for molten salt reactors, only two have been operated, both in the US between the 1950s and 60s, and gas-cooled and supercritical water reactors remain in the development phase.

1.1.3 Lead-cooled reactors. Passive cooling by natural convection

A particular advantage of designs featuring liquid metal cooling is that it allows for operating on a fast neutron spectrum while at the same time not needing significant pressurisation of the primary circuit. A fast neutron spectrum opens the possibility to operate with a breeding ratio[2]close larger than unity (in which case they are referred to as *fast breeders*[17]), leading to a dramatic improvement on fuel utilization efficiency. Fast reactors also can be designed to consume long-lived *minor actinides* (MA), a significant contributor to the radioactive and thermal output of spent nuclear fuel, making them furthermore able to reduce nuclear waste production.

On the other hand, operating the reactor at or close to atmospheric pressure carries a very significant advantage with respect to e.g. light water reactors, since it minimizes the increased design complexity and cost derived from both the need to contain the very high pressures involved, and from the engineered safety measures demanded to mitigate loss of pressure accidents.

As pointed above, modern designs involving liquid metal as coolant consider the use of either sodium, lead, or lead-bismuth. All of these materials have a sufficiently low melting point to be practical. More specifically, the use of liquid lead as coolant has some notable advantages, namely:

- *Chemical stability.* Lead does not share sodium's main drawback, that is, its high propensity to react exothermally upon contact with either water, e.g. from the secondary circuit, or even air, which require careful isolation of the coolant.

- *Natural convection.* The high gradient that lead's density features with respect to its temperature permits the use of entirely passive natural convection as a means of residual heat removal, which is proportional to that gradient (see Equation (2.24)), while maintaining reasonable reactor dimensions. This passive safety property is very attractive when compared to the need in conventional reactor designs to engineer means to actively extract residual heat; even when off-site, or even potentially on-site, power is lost, like in Fukushima.

- *High boiling temperature.* With a boiling point of over 1700 °C (over 800°C higher than sodium's), the loss of coolant by boiling, a concern that is front and center in LWR design, is essentially removed.

- *Shielding.* At the same time, lead's excellent shielding characteristics against ionizing radiation mean that using it as coolant will spare the reactor vessel from most of the neutron radiation damage that it would otherwise receive, extending its lifetime.

- *Fission product binding.* Furthermore, in the eventuality of of volatile fission product release as a result of cladding damage, lead readily forms stable compounds with iodine,

[2]The conventional definition of a breeder reactor is that which has a larger inventory of fissile material at the end of a fuelling cycle (EOL) than at the beginning of it (BOL). However, a more helpful definition for a reactor having a breeding ratio larger than one is provided in [16]: "The sum of reactivity changes during burn-up and subsequent cooling, reprocessing and re-fabrication of the fuel should be larger than zero." This definition is helpful because, unlike the former, it is the condition that must be satisfied in order for a reactor to be able to refuel using only its own spent fuel, together with the appropriate amount of fertile material.

cesium and polonium[3], which are retained within the coolant to a greater extent than the corresponding volatile elements[18, 19]. The former two are the two main isotopes of concern from a fission product release, when one takes into account both total inventory and radiotoxicty. Therefore, the magnitude of the source term is reduced when compared to that of a LWR under equivalent conditions.

On the other hand, the use of lead as coolant has some drawbacks, the main ones being:

- *Coolant freezing.* The comparatively higher melting point of pure lead (as opposed to lead-bismuth, or sodium) means that the entire system must be kept at a high enough temperature, including under reactor scram and refuelling or maintenance conditions. This requires the inclusion of heating elements and overall adds complexity to the design process.

- *Coolant mass.* The flip side of the high coolant density that makes it an excellent choice for passive convective cooling is that the total reactor mass is noticeably increased. This must be taken into account in the design, especially when considering seismic constraints.

- *Opacity.* An easy to overlook drawback, the opacity of lead makes it impossible to visually inspect core components during maintenance (indeed, its shielding characteristics even complicate non-invasive material inspection techniques such as x-ray or gamma probing).

- *Activation.* Albeit a limited concern when using only lead (as opposed to lead-bismuth), a small amount of radioactive polonium will be produced in the coolant[3].

- *Material corrosion.* Finally, the most important drawback of liquid lead cooling, and which has historically been the main roadblock to this technology, is the highly corrosive nature of lead in contact with steel. As a consequence, operation for any meaningful amount of time requires the formation of a stable protective oxide layer. With conventional steels, this would necessitate a very stringent control of oxygen levels at all points of the primary circuit[19], in order to guarantee the formation of said oxide layer but at the same time to avoid the formation of lead oxide precipitates that have hampered operation of lead-bismuth cooled cores in the past[20].

In this context, a potentially breakthrough innovation has been achieved during the last decade at the Royal Institute of Technology (KTH) in Stockholm. It involves the development of *alumina-forming steel* compounds (see [21, 22] and more recently [23, 24]). As the name indicates, this alloy, specifically Fe-10Cr-4Al-RE[4], is tuned to achieve the formation of a thin, stable, self-healing alumina (aluminum oxide) layer, which protects the bulk of the steel from corrosion in a much broader range of oxygen levels and temperatures up to 800 K. Research on these materials is presently ongoing to study their performance in the more complex situations required for their qualification in a nuclear application, such as broader temperature and oxygen level ranges,

[3] The radioactive isotope ^{210}Po is created by neutron capture of bismuth. This coolant activation is a more significant concern in the case of lead-bismuth eutectic (44.5% lead, 55.5% bismuth) coolant, which was used in Soviet submarine reactors and features a much lower melting point of 125°C. However, even the purest lead commercially available will contain bismuth in trace amounts.

[4] "RE" stands for "reactive elements"; trace amounts of Y, Zr, Ti, Hf, Ce, and Sc that are essential for the creation of thin, stable oxide layers by preventing the formation of chromium carbides that may be detrimental to corrosion resistance, while enabling the aluminium concentration to remain at a level low enough to ensure good weldability.

flowing lead conditions or neutron irradiation.

1.2 The SUNRISE project

The SUNRISE project (Sustainable Nuclear Research In Sweden)[25], managed by KTH, Luleå University of Technology, and Uppsala University was launched as a response to a call by the Swedish Foundation for Strategic Research (SSF) in 2020 with the goal of forming research centres "[...] on Future Advanced Technology for Sustainability" in various technology areas, in order to promote "research that meets the highest international scientific standing and promotes innovation [towards a] substantial impact on sustainable development within [...] a 10-15 year horizon"[26]. SUNRISE was granted SEK 50 million by the SSF.

Figure 1.2: "SUNRISE (Sustainable Nuclear Energy Research In Sweden) is the first step towards building a lead-cooled research and demonstration reactor in Sweden."[25]

The stated goal of SUNRISE is to carry out "design, safety analysis and materials development and qualification for a lead-cooled research reactor" to be built in Sweden. Various Swedish and international universities, regulators and industrial parters have a stake in SUNRISE. In addition to demonstrating the viability of LFR technology, such reactor will provide opportunities for materials and irradiation experiments, computational tool validation and verification, and student and professional training.

A subsequent SEK 99 million have been granted to the research group in early 2022 by the Swedish Energy Agency for the construction of an electrically powered prototype plant, dubbed Solstice, in Oskarsharm, in the south of Sweden[27]. In addition to the use of lead as a coolant, SUNRISE contemplates developing corrosion-resistant cladding alloys, as well as eventually qualifying novel uranium nitride (UN) fuel, which features a significantly larger thermal conductivity[28].

1.2.1 SEALER

In collaboration with SUNRISE, KTH spin-off company LeadCold[29] draws from the research and aims to commercialize compact lead-cooled, fast-spectrum reactor design SEALER (Swedish Advanced Lead Reactor).

The proposed system aims to reduce operational expense and minimize proliferation concerns by featuring a long (10-30 years) core life, so that no refuelling on site is necessary. This is possible by operating with a breeding ratio higher than 1 at BOL, so that a higher burn-up can be achieved; while at the same time reducing the reactivity swing over the lifetime of the core. This, in turn, reduces the need for control assemblies, which are withdrawn from the core at BOL.

SEALER takes advantage of the features of lead coolant listed above. SEALER is designed to be

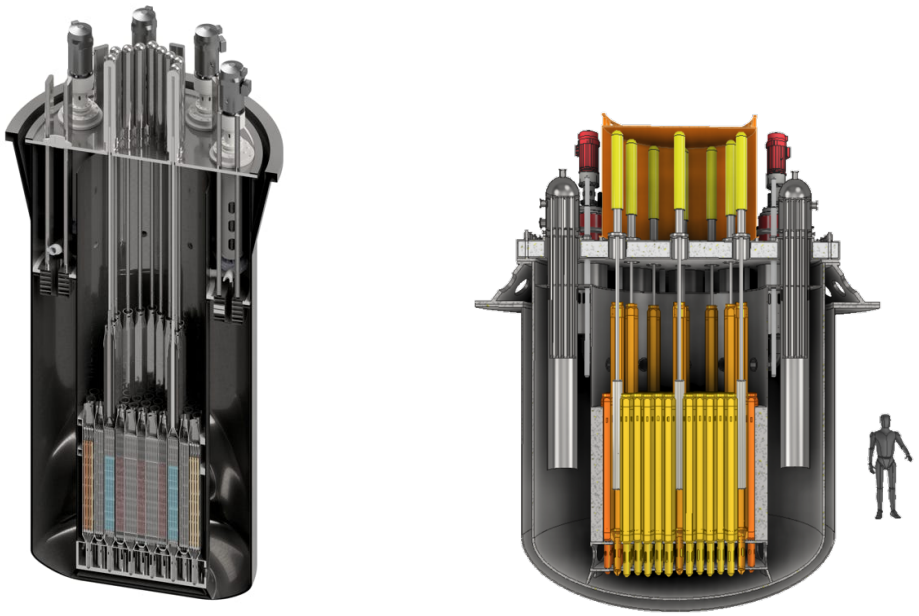

(a) SEALER-Arctic (b) SEALER-55

Figure 1.3: Two distinct SEALER designs are currently being developed.
SEALER-Arctic (*left*) is intended for remote Arctic communities, such as mining operations. Those communities are almost never connected to the grid, and are instead powered by diesel generators. It is fuelled with 2.4 tons of uranium oxide enriched at 19.9%, and intended for an electrical power output below 10 MW, giving it a core life of up to 30 years without refuelling.
SEALER-55 (*right*), with 55 MWe of nominal power, is designed to be eventually fuelled with 21 tons of 12% enriched UN and is intended for use in electrical grids, with the option of several units in the same power facility. Its planned full power core-life is 25 years.
Reactor schematics are provided by LeadCold[30] (not at the same scale).

passively safe through the removal of residual core heat by natural convection of the coolant. To that end, *dip-coolers*[5]are included in order to guarantee a heat sink to maintain the convective flow, should the steam generators become unavailable. Furthermore, upon failure of the dip-coolers, SEALER's power rating and dimensions are such that completely passive heat removal by thermal radiation from the reactor vessel would prevent that damage to the fuel. Finally, if volatile fission products were to be released, lead's inherent capacity of chemically binding such products would retain them within the reactor vessel, minimizing the source term to the exterior.

1.3 ADELE

The goal of this project is to develop and validate a *design code*, termed *ADELE* (Analytical DEsign of LEad-cooled reactors) in the form of a mobile application, for small, lead-cooled, fast spectrum nuclear reactors (LFR). The target user for this application is mainly students in the Nuclear Engineering field.

[5] At a high level, a dip-cooler is a heat exchanger system in which water is stored at an elevation and, when required, circulated through pipes inside the primary system. The system is dimensioned so that this circulation is entirely driven by natural circulation.

What is meant here by *design code* is that it is not the objective of this code to carry out very complex and detailed (and computationally costly) simulations of the reactor at the system level. Instead, its use case is to *facilitate the rapid exploration of the parameter space in the early design stages*. Therefore, the characteristics of *ADELE* are geared to such a purpose, so that the computational load is low enough for the application to run locally on mobile devices.

The development of *ADELE* draws, in significant part, from the BELLA code, developed by Sara Bortot *et al*[31] for the development of small LFRs. This code is actively used in the design work carried out within the aforementioned SUNRISE project at KTH.

The main characteristics of *ADELE* are the following:

- *Condensed parameters*. Also known as *lumped parameters*, the first way in which the computational cost is constrained is by condensing the physical characteristics of components to a point (i.e. a zero-dimensional model). Thus, the core is modelled with an *inlet* and an *outlet* temperatures, and the coolant velocity is taken as constant across the core, as two examples.

- *Analytical model*. Furthermore, the model of the reactor is entirely analytical. That is, no Monte Carlo simulations are performed, but instead the computations are limited to the solving of algebraic equations.

- *Core geometry*. In this work, the core is assumed to consist of a number of hexagonal fuel assemblies, in which the cylindrical fuel rods are separated using spacer wires; these assemblies are in turn arrayed on a hexagonal grid. This configuration is common for fast spectrum reactors, since it minimizes the distance between fuel rods, as compared to the square grid geometry habitual for thermal reactors.

  Additionally, the space for the central assembly in the core is left empty, following e.g. [18]. This flattens the neutron flux distribution, ameliorating the neutron leak that is always more significant in smaller cores, and furthermore prevents excessive burning of the assembly that would occupy that spot, since the goal is to avoid the need to reshuffle the fuel.

More specifically, the following conditions are imposed on the model in order to ensure a unique solution that can be reached analytically:

- *Natural convection cooling*. The reactor geometry must allow for the removal of all residual heat by means of natural circulation, and furthermore must do it while maintaining the nominal coolant inlet and outlet temperatures. This latter point is important since, in that way, the material integrity of the core components is ensured during a transient in which forced circulation is lost.

  Beyond that, it is imposed that the natural circulation must happen at a velocity high enough to guarantee a turbulent flow regime, in order to maintain sufficient mixing and thus an efficient heat removal capability.

- *Fuel temperature.* The nominal temperature profile of the peak fuel element must leave enough margin to allow for a hypothetical transient in which thermal power is allowed to increase up to twice the nominal value, without the center of the fuel reaching the

melting point. This power doubling transient assumption derives from the large security margins which are needed in research reactors like the SUNRISE-LFR (e.g. some kinds of unprotected transients must be able to be studied safely), within the framework of which this work was carried out.

- *Fission gas release.* The fuel rods must include an upper plenum large enough to accommodate a release of 100% of the gaseous fission products within the fuel, while keeping the pressure below a limit in order to guarantee the integrity of the cladding.

- *Minimum critical mass.* The smaller size, combined with the long refuelling time requirement, tends to make it advantageous to opt for a smaller fuel mass and a larger enrichment (see Figure 1.3). In *ADELE*, the conditioned imposed is that, of those configurations that provide the required thermal power while appropriately cooling the fuel rods, that with the minimum number of fuel rods, with the smallest diameter, is chosen. The enrichment is then tuned so that the core is critical (recalling that, in the reactor in question, the breeding ratio is larger than unity at BOL and thus the control rods are fully extracted, as reactivity will increase, not decrease, in the first phase of the fuelling cycle).

These conditions are developed analytically in the following sections in some detail. The full derivations can be found in Appendix B.

ADELE is developed within this project as an application for the iOS operating system, and using the programming language SwiftUI[32]. This work was carried out in the course of an internship at KTH.

2 Analytical model

There are two people in a wood, and they run into a bear.
The first person gets down on his knees to pray;
the second person starts lacing up his boots.
The first person asks the second person,
"My dear friend, what are you doing? You can't outrun a bear."
To which the second person responds,
"I don't have to. I only have to outrun you."
— *Benedict Cumberbatch, in The Imitation Game (2014)*

2.1 Introduction

The analytical modelling of the core in this work is pursued via a *hybrid* approach. What is meant by this is that the core is studied, at times, as a *homogeneous cylindrical reactor*; while in others, the heterogeneous geometry of the fuel pins and the coolant channels is taken into account.

A hexagonal fuel assembly is schematically depicted in Figure 2.1a. It consists of cylindrical fuel rods, arranged in a hexagonal pattern and featuring spacer wires, which wrap around the fuel pins to keep them at a constant distance from each other. It is noted that different geometries of cooling channels are present in such an assembly, termed *interior*, *edge* and *corner* channels. As will be expanded upon later, for the purposes of this work only the interior channels are going to be modelled (Figure 2.1b), and the properties of the entire assembly, and by extension of the whole core, are going to be extrapolated from them. The error introduced by this simplification is considered acceptable, given that thousands of coolant channels are expected (and thus a large majority of the coolant mass within the core will be flowing along these internal channels), and given the other approximations taken overall in the model.

On the other hand, when using a homogeneous approximation to characterize the core, a cylindrical geometry is assumed, as illustrated in Figure 2.2. Furthermore, this homogeneous cylindrical reactor is going to be characterised as having an *active height* (the height of the pins corresponding to the fuel) equal to its diameter. These proportions guarantee the lowest surface-to-volume ratio, and therefore an optimized neutron economy.

A consequence of those two separate approaches is that special care must be paid to ensure that consistency is maintained between parameters that may be computed independently. This is the case of the core active height, H_f, and the fuel pin diameter, D. As shown in latter sections, they are obtained using separate assumptions. It is therefore necessary to ensure that the total

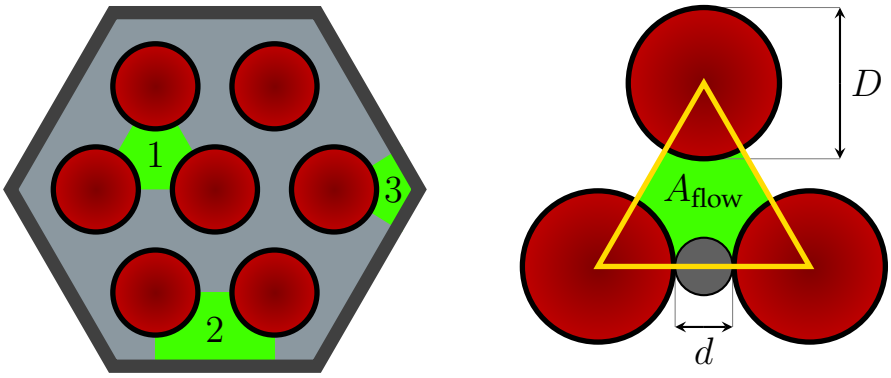

(a) (b)

Figure 2.1: *Left:* A generic fast reactor hexagonal fuel assembly, featuring internal triangular channels (1) as well as *edge* and *corner* channels (2,3). *Right:* Triangular coolant flow channel within a hexagonal fuel assembly, featuring a spacer wire.

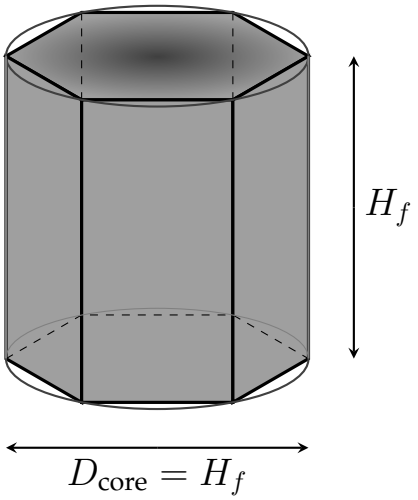

Figure 2.2: Schematic of the active core, which is modelled as a homogeneous cylinder with a height equal to its diameter.

cross-section of the fuel pins is consistent with the core cross-section, i.e. that the fuel "fits" in the core. Specifically, the cross-section area of the cylindrical core, A_{core}, is

$$A_{\text{core}} = \frac{\pi}{4} {H_f}^2 \tag{2.1}$$

And, given a total number of fuel rods within the core of N_{rod}, the total fuel cross-section A_{fuel} corresponds to

$$A_{\text{fuel}} = \frac{\pi}{4} D^2 N_{rod} \tag{2.2}$$

Therefore, dividing Equation (2.1) by Equation (2.2) gives the fraction of the core occupied by fuel:

$$\frac{A_{\text{fuel}}}{A_{\text{core}}} = \frac{D^2\, N_{rod}}{{H_f}^2} \tag{2.3}$$

Which must remain below a prescribed fraction, lower than unity.

2.2 Neutron flux. Criticality

For the purpose of modelling the neutron flux in the reactor, the homogeneous cylindrical reactor presented above (Figure 2.2), in which the fuel mass is uniformly distributed within the core volume, is used.

Furthermore, it is assumed that all the neutrons to have a uniform energy, in other words, they are considered to be in a single *energy group*. This allows for the modelling of the neutron flux using the relatively straightforward one-group diffusion theory.

The obvious drawback with assuming mono-energetic neutrons is that it generally tends to result in, at best, very rough estimates for magnitudes like the multiplication factor and the critical mass. However, it is important to note that this improves significantly when dealing with fast neutron reactors, as in this case, since the main problem with the one-group theory, namely that it does not consider the role of moderation and thermal neutrons, is much less relevant when considering only fast fission. On the flip side, it significantly streamlines the computations associated, without introducing a disproportionate error when compared to the rest of the approximations taken overall.

When using the homogeneous reactor approximation, it becomes apparent that a bare cylindrical reactor is not an adequately realistic model; yielding results far too inaccurate for this purpose. Instead, a reflected reactor is adopted as the model. This is consistent with the lead coolant surrounding the core being an excellent neutron reflector.

However, solving the diffusion equation for a reflected, finite cylinder is quite complex[1]. Fortunately, empirically it is found that the neutron flux shape (and therefore the buckling) *inside the core* in the reflected case is quite similar to that for the bare case, as long as one adjusts for a larger *extrapolated length*. This is not a trivial claim, and must be kept in mind when validating the results.

Specifically, then, the neutron flux distribution within the core, ϕ, is taken as the well known expression for a bare, finite cylinder of extrapolated radius $\tilde{R}$ and extrapolated height $\tilde{Z}$ (see Appendix B for an outline of the derivation, reproduced from [33]):

$$\phi(r,z) = A\, J_0\left(\frac{2.405\, r}{\tilde{R}}\right) cos\left(\frac{\pi z}{\tilde{Z}}\right) \quad \text{with} \quad r \in (0,\tilde{R})\,; \quad z \in \left(-\frac{\tilde{Z}}{2}, \frac{\tilde{Z}}{2}\right) \tag{2.4}$$

[1] To the author's knowledge, the diffusion equation for a finite, reflected cylindrical reactor is not solved in the literature, neither for the one- nor the multi-group case. Mathematically it requires the introduction of *modified Bessel functions*, since the diffusion equation in the reflector medium (no neutron source) solves for a linear combination of Bessel functions evaluated at pure imaginary values.

Where J_0 is the *Bessel function of the first kind of order zero*, and A is a free constant that can be set knowing the total power of the reactor (the diffusion equation is homogeneous and thus a real multiple of a solution is also a solution); it is not computed here because the neutron flux is not strictly needed in this work, but only the *buckling*, or square of the first eigenvalue of the solution, namely

$$B^2 = \left(\frac{2.405}{\tilde{R}}\right)^2 + \left(\frac{\pi}{\tilde{Z}}\right)^2 \tag{2.5}$$

and where the extrapolated dimensions due to the core being reflected are found empirically to correspond to about 50% larger a value when compared to those of the active core itself, H_f and $R_0 = H_f/2$; that is, then,

$$\tilde{H} = \frac{3}{2} H_f \; ; \qquad \tilde{R} = \frac{1}{2}\left(\frac{3}{2} \cdot H_f\right) = \frac{3}{4} H_f \tag{2.6}$$

With that, the multiplication factor k can be obtained as a function of, among other things, the fuel enrichment e. To that end, the *one-group reactor equation* is expressed as (see [33]):

$$\boldsymbol{k = \frac{\nu \Sigma_f}{D B^2 + \Sigma_a}} \tag{2.7}$$

Where ν is the fission yield, or neutrons per fission; D corresponds to the diffusion coefficient (units of length) from Fick's law; Σ_f and Σ_a correspond respectively to the macroscopic fission and absorption cross-sections; and B^2 is the buckling, which is expressed in Equation (2.5).

The relevant nuclear reactions taken into account for the reactor equation are:

- Fission of ^{235}U and ^{238}U
- Neutron capture by ^{235}U, ^{238}U and the cladding, modeled to this end as iron metal (neutron capture by the coolant has a negligible effect on neutronics and is not considered here)

To compute the associated macroscopic cross sections, then, atom densities of ^{235}U, ^{238}U and Fe in the core are obtained (in units of m^{-3}):

$$N^{235} = N^{235}_{\text{fuel}} \frac{V_{\text{fuel}}}{V_{\text{core}}} = e\, N^{\text{U}}_{\text{fuel}} \frac{V_{\text{fuel}}}{V_{\text{core}}} = e\, \frac{\rho_f N_A}{M_{\text{UO}_2}} \frac{D^2_{\text{pellet}}\, N_{rod}}{{H_f}^2} \tag{2.8}$$

$$N^{238} = (1-e)\, \frac{\rho_f N_A}{M_{\text{UO}_2}} \frac{D^2_{\text{pellet}}\, N_{rod}}{{H_f}^2} \tag{2.9}$$

$$N^{\text{clad}} = N^{\text{Fe}}_{\text{clad}} \frac{V_{\text{rod}}}{V_{\text{core}}} = \frac{\rho_{\text{clad}}\, N_A}{M_{\text{clad}}} \text{CTR}(2 - \text{CTR}) \frac{D\, N_{rod}}{{H_f}^2} \tag{2.10}$$

Where, as previously, D is the fuel rod diameter (i.e. the cladding outer diameter) and CTR is the *cladding thickness ratio*, a dimensionless parameter, commonly used in rector design, that corresponds to the ratio between the thickness, t_{clad}, and the (average) diameter, D, of the cladding[2]:

$$\text{CTR} = \frac{t_{\text{clad}}}{D} \tag{2.11}$$

In this way, the macroscopic cross sections are derived from these:

$$\Sigma_f = \Sigma_f^{235} + \Sigma_f^{238} = N^{235}\sigma_f^{235} + N^{238}\sigma_f^{238} \tag{2.12}$$

$$\Sigma_c = \Sigma_c^{235} + \Sigma_c^{238} + \sigma_c^{\text{clad}} = N^{235}\sigma_c^{235} + N^{238}\sigma_c^{238} + N^{\text{clad}}\sigma_c^{\text{clad}} \tag{2.13}$$

And

$$\Sigma_a = \Sigma_f + \Sigma_c \tag{2.14}$$

As for the diffusion coefficient, it is obtained from the diffusion area, L^2:

$$D = \Sigma_a \, L^2 \tag{2.15}$$

The diffusion area and the microscopic cross-sections are constant parameters in the model. They are obtained from Monte Carlo simulations carried out in the course of the design of SEALER and otherwise within the SUNRISE project.

2.3 Fission gas pressure. Cladding stress

In a solid-fuel nuclear reactor, when an atom undergoes fission, the resulting nuclei remain confined within the fuel pellet. A fraction of these fission products will be gasses (isotopes of krypton and xenon being the most relevant in the case of uranium fuel), which accumulate as the fuel is burned. These gaseous fission products may be released into the fuel rod plenum in case of damage to the fuel pellets, either following a transient or as a result of defect accumulation during the fuel's lifetime.

In the following section, the height of the fuel rod plena, and thus of the fuel rod as a whole, is characterised. This height needs to be minimized, to avoid excessive pressure losses in the flow of the coolant; while being large enough to accommodate the release of the gaseous fission products from the fuel, without the pressure caused by their release resulting in excessive stress on the fuel cladding.

[2]For the rest of this work, this ratio is fixed at CTR $= 0.05$, i.e. the thickness of the cladding is taken to be $t_{\text{clad}} = D/20$.

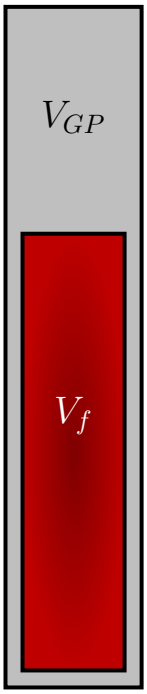

Figure 2.3: Diagram of a cross-section of a fuel rod (not to scale), featuring the fission gas plenum.

Conservatively, the rod plenum height is computed assuming a release of the entire inventory of fission gasses (FG) from the fuel, taking place at EOL. To compute the magnitude of this inventory, the number density of uranium atoms in solid UO_2 fuel, n_U (mol/m^3), is first computed:

$$n_{\mathrm{U}} = \left(\frac{\text{mol U}}{\text{mol UO}_2}\right) \cdot \left(\frac{\text{mol UO}_2}{\text{kg UO}_2}\right) \cdot \left(\frac{\text{kg UO}_2}{\text{m}^3\ \text{UO}_2}\right) = 1 \cdot \frac{1}{M_{\mathrm{UO}_2}} \cdot \rho_f \tag{2.16}$$

with ρ_f being the mass density of the fuel, and $M_{\mathrm{UO}_2} = 0.270$ kg/mol being the molar mass of uranium oxide. From this, the total fission gas inventory (in mol) in one fuel rod is obtained, by taking into account that the average yield of xenon and krypton from this type of fuel is $Y_{FG} = 0.25$ atoms per fission, and assuming a burn-up of $BU_{\%}$ representing the fraction of uranium atoms that do undergo fission, given a total fuel volume within the rod V_f:

$$n_{FG} = n_{\mathrm{U}} \cdot Y_{FG} \cdot BU_{\%} \cdot V_f = \frac{\rho_f\, Y_{FG}\, BU_{\%}\, V_f}{M_{\mathrm{UO}_2}} \tag{2.17}$$

From which the pressure that the fission gas release exerts within the rod plenum volume V_{GP} is obtained using the ideal gas law:

$$p_{FG} = \frac{n_{FG}\, R\, T_{FG}}{V_{GP}} = \frac{V_f}{V_{GP}} \frac{R\, Y_{FG}}{M_{\mathrm{UO}_2}} \rho_f\, BU_{\%}\, T_{FG} \tag{2.18}$$

Where T_{FG} is the temperature of the plenum. In turn, the pressurization of the fuel rod plenum

by the fission gasses induces a tangential stress on the cladding, known as *hoop stress*. For a case of thin-walled hollow cylinders, such as a fuel rod cladding, this hoop stress can be approximated by the following expression:

$$\sigma_h = \frac{r_{\text{clad}}}{t_{\text{clad}}} p_{FG} \tag{2.19}$$

As a reference value, the maximum allowable hoop stress for 15-15Ti, a standard material of fast reactor cladding, is of $\boldsymbol{\sigma_h^{max} = 200}$ MPa. Furthermore, it is useful to rewrite the expression above in terms of the cladding thickness ratio, CTR, exposed previously:

$$\frac{1}{p_{FG}} = \frac{D/2}{t_{\text{clad}}} \frac{1}{\sigma_h} = \frac{1}{2\,\text{CTR}\,\sigma_h} \tag{2.20}$$

Thus, applying (2.20), equation (2.18) can be rewritten to express the minimum volume for the rod plenum, given this maximum stress value and its relation with the plenum pressure expressed in (2.20):

$$V_{GP} = V_f \frac{R\,Y_{FG} BU_{\%}}{2\,M_{\text{UO}_2}} \frac{\rho_f\,T_{FG}}{\text{CTR}\,\sigma_h^{max}} \tag{2.21}$$

Next, given that the cross-sections of the gas plenum and the fuel are nearly equal (neglecting, therefore, the contribution of the gap between the cladding and the fuel to the total free volume inside of the rod), both sides of equation (2.21) are divided by this cross-sectional area:

$$H_{GP} = H_f \frac{R\,Y_{FG} BU_{\%}}{2\,M_{\text{UO}_2}} \frac{\rho_f\,T_{FG}}{\text{CTR}\,\sigma_h^{max}} \tag{2.22}$$

From which a closed expression for the height of the fuel rod, H_{ch}, is obtained:

$$\boldsymbol{H_{ch} = H_f + H_{GP} = H_f \left(1 + \frac{R\,Y_{FG} BU_{\%}}{2\,M_{\text{UO}_2}} \frac{\rho_f\,T_{FG}}{\text{CTR}\,\sigma_h^{max}}\right)} \tag{2.23}$$

2.4 Natural convection

Another one of the primary conditions imposed in the design is that the resulting reactor must be able to dissipate all of its residual heat by means of natural convection alone. This guarantees passive safety as long as the heat sink, in the form of the dip-cooler, is available.

In practise, this condition is met if the *buoyancy head*, or pressure difference due to the change in density associated with temperature, equals the pressure drop along the coolant path.

The buoyancy head is expressed as

$$\Delta p_{\,\text{buoyancy}} = g\left(\rho_{Pb}(T_{in}) - \rho_{Pb}(T_{out})\right) H_{DC} = g\,\Delta\rho_{Pb}(\Delta T)\,H_{DC} \tag{2.24}$$

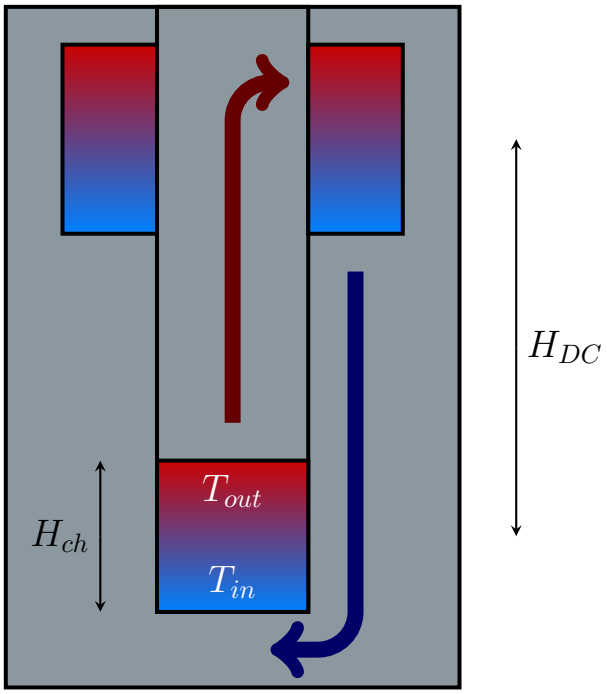

Figure 2.4: Schematic depicting the flow of coolant driven by natural convection, with the dip-coolers (top) acting as the heat sink.

Where H_{DC} corresponds to the elevation of the dip-cooler above the core, and $\Delta\rho_{Pb}(\Delta T)$ is the difference in coolant density at the core inlet and the outlet temperatures, T_{in} and T_{out}. The density difference is deliberately expressed as depending explicitly on the temperature difference ΔT, as $\rho_{Pb}(T)$ is assumed linear in the relevant temperature range (all correlations used in this work are detailed in Appendix A). The values of T_{in}, ΔT and H_{DC} are input into the model by the user, the latter corresponding with the highest elevation of the dip-cooler consistent with construction and seismic constraints.

In particular, note that ΔT is taken to be the same under both nominal and convective conditions, i.e. it is imposed that the passive removal of residual heat must be effective enough not to lead to a temperature increase upon loss of forced circulation.

As for the pressure losses under natural circulation conditions, Δp_{nat}, it is taken to be proportional to the pressure drop along the core channels, for which the Darcy-Weisbach empiric formula is used:

$$\Delta p_{\text{nat, total}} = K \cdot \Delta p_{\text{nat, channel}} = K f_{nat} \frac{H_{ch}\, \rho_{Pb}\, {v_{nat}}^2}{2 D_h} \tag{2.25}$$

Where H_{ch} corresponds to the length of the coolant channel, i.e. the fuel pin height; v_{nat} the coolant velocity under natural convection, D_h the core's hydraulic diameter; and the density of the coolant, ρ_{Pb}, is taken, from here on forward, to be computed at the coolant's average temperature within the core, consistent with the lumped parameter approach, which is simply

$$T_{Pb} = T_{in} + \frac{\Delta T}{2} \tag{2.26}$$

The simplification taken in Equation (2.25), in which the proportionality factor is taken to be $\boldsymbol{K = 1.5}$, assumes that the other pressure drops not directly consequence of friction losses in the channel (e.g. due to changes in cross-section at the inlet and the outlet of the core) are also approximately proportional to the velocity squared.

As for the Darcy friction factor f, it is assumed to correlate to the Reynold's number (and therefore the flow velocity) as expressed by the classical Blasius formulation:

$$f = a \cdot \mathrm{Re}^{-b} = a \left(\frac{\rho \, v \, D_h}{\mu} \right)^{-b} \tag{2.27}$$

With μ the (dynamic) viscosity of the fluid. This expression is then fitted, following Dehlin *et al.*[34], to Cheng and Todreas's correlation obtained specifically for hexagonal fuel elements with wire spacers[35]. This allows for the analytically simpler expression of Equation (2.27) to be used while keeping an acceptably low relative error (below 10% in the range of interest). The fitting parameters are taken as $\boldsymbol{a = 0.406}$ and $\boldsymbol{b = 0.272}$.

Thus, imposing that natural circulation is established under the nominal temperature difference corresponds to equating the buoyancy head to the pressure losses at the corresponding coolant velocity, i.e. equating expressions (2.24) and (2.25):

$$g \, \Delta\rho_{Pb}(\Delta T) \, H_{DC} = K f_{nat} \frac{H_{ch} \, \rho_{Pb} \, {v_{nat}}^2}{2 D_h} \tag{2.28}$$

On the other hand, an expression analogous to (2.25) can be written to express the pressure losses of the coolant under nominal conditions:

$$\Delta p_{nom} = K f_{nom} \frac{H_{ch} \, \rho_{Pb} \, {v_{nom}}^2}{2 D_h} \tag{2.29}$$

Then, by equating the value of hydraulic diameter D_h under both flow conditions as expressed in equations (2.28) and (2.29) one obtains the following expression:

$$D_h = K f_{nat} \frac{H_{ch} \, \rho_{Pb} \, {v_{nat}}^2}{2g \, \Delta\rho_{Pb}(\Delta T) \, H_{DC}} = K f_{nom} \frac{H_{ch} \, \rho_{Pb} \, {v_{nom}}^2}{2 \Delta p_{nom}} \tag{2.30}$$

Which is then solved for the nominal pressure loss:

$$\Delta p_{nom} = \frac{f_{nom}}{f_{nat}} \left(\frac{v_{nom}}{v_{nat}} \right)^2 g \, \Delta\rho_{Pb}(\Delta T) \, H_{DC} = \left(\frac{v_{nom}}{v_{nat}} \right)^{2-b} g \, \Delta\rho_{Pb}(\Delta T) \, H_{DC} \tag{2.31}$$

Where the form of the friction factor from Equation (2.27) has been applied. Finally, an expression for the nominal pressure losses that does not depend explicitly on flow velocities is reached by realizing that, assuming no change in fuel temperature, energy conservation mandates that flow velocity is proportional to the total extracted thermal power $\dot{Q}$:

$$\dot{Q} = \dot{m}_{Pb}\, c_p\, \Delta T = \rho_{Pb}\, \mathcal{A}_{\text{flow}}\, v\, c_p\, \Delta T \tag{2.32}$$

where $\mathcal{A}_{\text{flow}}$ is, in this case, the *total* cross-sectional area of the coolant flow, and is c_p the specific heat of the coolant; and that therefore the ratio of velocities from equation (2.31) can be written as

$$\frac{\boldsymbol{v_{nat}}}{\boldsymbol{v_{nom}}} = \frac{\boldsymbol{\dot{Q}_{res}}}{\boldsymbol{\dot{Q}_{nom}}} \tag{2.33}$$

where $\dot{Q}_{res}/\dot{Q}_{nom}$ is the fraction of nominal power that is expected after reactor shutdown, which is to be removed by natural convection; and which is one of the parameters introduced to the model by the user.

Therefore, substituting (2.33) into (2.31) yields the following expression for the nominal pressure losses:

$$\boldsymbol{\Delta p_{nom}} = \boldsymbol{g\, \Delta \rho_{Pb}(\Delta T)\, H_{DC}} \left(\frac{\boldsymbol{\dot{Q}_{res}}}{\boldsymbol{\dot{Q}_{nom}}} \right)^{\boldsymbol{b-2}} \tag{2.34}$$

One more condition that is necessary in order to close the system of equations is to impose that the velocity in the convective regime, v_{nat}, be high enough to guarantee a turbulent flow along the core channels. That is, the minimum natural convection velocity is taken to be so that the Reynolds number is above a given threshold:

$$\text{Re}_{nat} = \frac{\rho_{Pb}\, v_{nat}\, D_h}{\mu_{Pb}} > \text{Re}_{nat}^{min} \tag{2.35}$$

Note that, in practise, the natural convection velocity will be fixed at this minimum threshold, as doing so also minimizes the nominal coolant velocity (since as shown in Equation (2.33) they are directly proportional) and thus minimizes both the damage to the core components and the pressure losses in the coolant flow. That is, v_{nat} is taken as

$$v_{nat} = \frac{\text{Re}_{nat}^{min}\, \mu_{Pb}}{\rho_{Pb}\, D_h} \tag{2.36}$$

The minimum Reynolds number in order to guarantee turbulent flow is conservatively set at $\text{Re}_{\boldsymbol{nat}}^{\boldsymbol{min}} = \mathbf{3600}$ by default, following [34], although it remains a parameter that the user may modify.

Computing v_{nat} from (2.36) requires an expression for D_h. This can be obtained from Equation (2.30) (natural convection term), in which the friction factor from (2.27) is substituted:

$$D_h = K \cdot a \left(\frac{\rho_{Pb}\, v_{nat}\, D_h}{\mu_{Pb}} \right)^{-b} \cdot \frac{H_{ch}\, \rho_{Pb}\, {v_{nat}}^2}{2g\, \Delta\rho_{Pb}(\Delta T)\, H_{DC}} \tag{2.37}$$

This is solved for D_h, yielding:

$$\boldsymbol{D_h = \left(\frac{aK H_{ch}}{2g\, \Delta\rho_{Pb}(\Delta T)\, H_{DC}} {\rho_{Pb}}^{1-b}\, {v_{nat}}^{2-b}\, {\mu_{Pb}}^{b} \right)^{1/1+b}} \tag{2.38}$$

And by substituting (2.38) into (2.36) and rearranging, one obtains the following expression for the coolant velocity in the natural convection regime:

$$\boldsymbol{{v_{nat}}^3 = \mu_{Pb} \left(\mathrm{Re}_{nat}^{min} \right)^{1+b} \frac{2g\, \Delta\rho_{Pb}(\Delta T)}{aK {\rho_{Pb}}^2} \frac{H_{DC}}{H_{ch}}} \tag{2.39}$$

2.5 Coolant channels. Fuel geometry

Drawing from the approach followed in Qvist *et al.*[36], one key for the analytical model used here is the realization that there are two separate ways to describe a coolant flow channel within a fuel assembly; namely, one that is based on thermal-hydraulics and another one, solely on geometry.

To obtain analytical expressions for the fuel rod and spacing wire diameters, the definition of hydraulic diameter in a flow channel of uniform cross-section is used as a starting point:

$$D_h = \frac{4A_{\text{flow}}}{P_{\text{wet}}} \tag{2.40}$$

Where A_{flow} is the cross-sectional area of one fuel element coolant channel, and P_{wet} corresponds to the *wetted perimeter*, or total length of material in contact with coolant within the cross-section. By recalling the triangular geometry of a cooling channel in a hexagonal fuel assembly shown in Figure 2.1b, with D and d being, respectively, the fuel rod and spacing wire diameters, the wetted perimeter and the channel flow area are directly obtained:

$$P_{\text{wet}} = 3 \cdot \frac{\pi}{6} D + \frac{\pi}{2} d = \frac{\pi}{2} (D + d) \tag{2.41}$$

$$A_{\text{flow}} = \frac{\sqrt{3}}{4} (D + d)^2 - \frac{\pi}{8} (D^2 + d^2) \tag{2.42}$$

Then, Equations (2.41) and (2.42) can be substituted into (2.40) to express the hydraulic diameter in terms of the diameters D and d:

$$D_h = \frac{2\sqrt{3}(D+d)^2 - \pi(D^2+d^2)}{\pi(D+d)} \tag{2.43}$$

Equations (2.42) and (2.43) effectively form a system of equations that allow for the expressing of D and d in terms of D_h and A_{flow}. Indeed, they can be shown to be the roots of a second-order polynomial:

$$\boldsymbol{D} = \frac{\boldsymbol{4}}{\boldsymbol{\pi}}\left[\frac{\boldsymbol{A}_{\text{flow}}}{\boldsymbol{D_h}} + \sqrt{\left(\frac{\boldsymbol{A}_{\text{flow}}}{\boldsymbol{D_h}}\right)^{\boldsymbol{2}}\left(\frac{\boldsymbol{4\sqrt{3}}}{\boldsymbol{\pi}} - \boldsymbol{1}\right) - \frac{\boldsymbol{\pi}}{\boldsymbol{4}}\boldsymbol{A}_{\text{flow}}}\right] \tag{2.44a}$$

$$\boldsymbol{d} = \frac{\boldsymbol{4}}{\boldsymbol{\pi}}\left[\frac{\boldsymbol{A}_{\text{flow}}}{\boldsymbol{D_h}} - \sqrt{\left(\frac{\boldsymbol{A}_{\text{flow}}}{\boldsymbol{D_h}}\right)^{\boldsymbol{2}}\left(\frac{\boldsymbol{4\sqrt{3}}}{\boldsymbol{\pi}} - \boldsymbol{1}\right) - \frac{\boldsymbol{\pi}}{\boldsymbol{4}}\boldsymbol{A}_{\text{flow}}}\right] \tag{2.44b}$$

To explicitly compute D and d, then, independent expressions for A_{flow} and D_h are needed. For the hydraulic diameter, Equation (2.38), derived in the previous section, is used. To obtain the coolant channel area, it is used once more that for any coolant channel with a constant cross-section, conservation of energy dictates the relation between the flow rate, $\dot{m} = A_{\text{flow}}\, v\, \rho$, and the extracted power within that channel, $\dot{Q}_{ch}$: under nominal conditions, they relate as

$$\dot{Q}_{ch} = \dot{m}_{Pb}\, c_p\, \Delta T = A_{\text{flow}}\, v_{nom}\, \rho_{Pb}\, c_p\, \Delta T \tag{2.45}$$

Just as exposed in Equation (2.32), but referring in this case to a single channel instead of to the core as a whole.

On the other hand, one may obtain an expression for the average thermal power extracted in a channel as a function of the total thermal power of the reactor, $\dot{Q}_{nom}$:

$$\dot{Q}_{ch,\,\text{mean}} = \frac{\dot{Q}_{nom}}{N_{ch}} = \frac{\dot{Q}_{nom}}{2\, N_{rod}} \tag{2.46}$$

I.e. $\dot{Q}_{ch,\,\text{mean}}$ corresponds to the fraction of the thermal power cooled by each of the channels, in average; and it is assumed that the number of channels relates to the total number of fuel pins in the reactor, N_{rod}, as $N_{ch} = 2\, N_{rod}$. This is not strictly true, since it extrapolates the ratio between fuel rods and coolant channels from the interior channels to the entire core and thus neglects the different cooling from exterior and edge channels (see Figure 2.1a); this approximation is consistent with the approach taken in the previous sections and is assumed to introduce and acceptably low error to the model.

As exposed in the introduction of the analytical method, and as Section 2.7 expands upon, the model uses as a constraint the peak temperature reached by the fuel during a hypothetical power doubling transient. Therefore, it is of interest to model the *peak* assembly, or assembly which sustains the most power. Therefore, a *radial peaking factor* F_R is introduced, which corresponds

to the ratio between the peak and the mean values for the thermal power. Hence, it follows that the value for the power extracted by the peak assembly is

$$\dot{Q}_{ch,\,\text{peak}} = F_R\,\dot{Q}_{ch,\,\text{mean}} = \frac{F_R\,\dot{Q}_{nom}}{2\,N_{rod}} \tag{2.47}$$

And subsequently, one obtains an expression for the flow area of the peak cooling channel by substituting (2.47) into (2.45):

$$\boldsymbol{A_{\text{flow}} = \frac{\dot{Q}_{ch,\,\text{peak}}}{\rho_{Pb}\,v_{nom}\,c_p\,\Delta T} = \frac{F_R\,\dot{Q}_{nom}}{2\,N_{rod}\,\rho_{Pb}\,v_{nom}\,c_p\,\Delta T}} \tag{2.48}$$

2.6 Fuel assembly pitch

A relevant and not directly intuitive point regarding the value of the fuel assembly pitch, p, is described next.

If one adds together the values obtained for the diameters of the fuel rod and the spacer wire in (2.44), the pitch is immediately obtained:

$$p = D + d = \frac{8}{\pi}\frac{A_{\text{flow}}}{D_h} \tag{2.49}$$

As before, for the numerator, the flow area is obtained from thermal-hydraulic considerations in Equation (2.48); while the hydraulic diameter as a function of the natural convection velocity is expressed in Equation (2.38). Therefore, by substituting (2.38) and (2.48) into (2.49), the following expression is obtained:

$$p = \frac{8}{\pi}\frac{\dfrac{F_R\,\dot{Q}_{nom}}{2\,N_{rod}\,\rho_{Pb}\,v_{nom}\,c_p\,\Delta T}}{\left(\dfrac{aK\,H_{ch}}{2g\,\Delta\rho_{Pb}(\Delta T)\,H_{DC}}{\rho_{Pb}}^{1-b}\,{v_{nat}}^{2-b}\,{\mu_{Pb}}^{b}\right)^{1/1+b}} \tag{2.50}$$

Which, after rearranging (see Appendix B for the full derivation), and using Equations (2.33) and (2.39), yields the following equation for the fuel assembly pitch:

$$\boldsymbol{p = \frac{4}{\pi}\frac{F_R\,\dot{Q}_{nom}}{N_{rod}\,c_p\,\Delta T}\frac{1}{\mu_{Pb}\,Re_{nat}^{min}}\left(\frac{\dot{Q}_{res}}{\dot{Q}_{nom}}\right)} \tag{2.51}$$

Remarkably, the pitch does not depend itself on other computed quantities of the model, such as the height of the fuel pins or the coolant velocity, which cancel out in the derivation. As is detailed in latter sections, this fact allows for a more straightforward computation of the reactor parameters, by first computing p separately and then using this to obtain the rest of the geometrical values.

2.7 Fuel temperature

A further condition that is imposed in this analytical approach is a constraint on the linear power rating of the reactor. Specifically, the total number of fuel rods, and their diameter (and thus the pellet size and the cladding thickness), are set in order to *i*) minimize the pressure losses and neutron leakage, while *ii*) guaranteeing sufficient cooling of the fuel to avoid melting in the hottest rod of the assembly during a transient doubling of the nominal thermal power.

Given a total number of fuel rods in the core N_{rod}, and a nominal thermal power $\dot{Q}_{nom}$, the nominal mean linear power $\overline{\chi}$ is

$$\overline{\chi} = \frac{\dot{Q}_{nom}}{N_{rod}\, H_f} \tag{2.52}$$

from which the peak linear power, χ_{peak}, is obtained. This value corresponds to the point in the reactor where the thermal power is highest (i.e. the center, see Section 2.2):

$$\chi_{\text{peak}} = F_R\, F_Z\, \overline{\chi} \tag{2.53}$$

F_R and F_Z being, respectively, the radial and axial peaking factors; indeed, the product $F_Z F_R = \Omega$ is the ratio between the power at the center of the core and the average value. The default values taken for this work are $F_R = 1.3$ and $F_Z = 1.2$[3].

It follows that, during a power doubling transient, the linear power at the peak location will be

$$\chi_{\text{peak, transient}} = 2\, F_R\, F_Z\, \overline{\chi} \tag{2.54}$$

On the other hand, the temperatures in the fuel pellet center line (*fc*), fuel pellet surface (*fs*), inner and outer cladding surfaces (*ci* and *co*), given a linear power value χ are related by the following set of equations.

The temperature difference between the lead coolant and the outer surface of the cladding is given by

$$T_{co} - T_{Pb} = \frac{D_h}{\pi D} \frac{\chi}{\lambda_{Pb}(T_{Pb})\, \text{Nu}_{Pb}} \tag{2.55}$$

Where D is the fuel rod outer diameter; λ_{Pb} corresponds to the thermal conductivity of the coolant (in W m^{-1} K^{-1}), evaluated at the average coolant temperature T_{Pb}; and Nu_{Pb} refers to the Nusselt number of the coolant flow under nominal conditions, which is for this work

[3] While the radial peaking factor of $F_Z = 1.2$ is obtained from the flux distribution, for F_R the analytical value is about 1.41 (see Appendix B). However, the aforementioned absence of the middle fuel assembly has a significant effect on flattening the power distribution; the empirical value of 1.3 is used instead.

computed using a correlation with other non-dimensional fluid parameters (all the correlations used can be found in Appendix A).

Subsequently, the following expressions yield the remaining temperatures of interest in the fuel pin. They are obtained by imposing a steady state (no time-dependent terms) on the heat equations for a straight, infinite cylinder (for the fuel pellet) or cylindrical shell (for the cladding and the cladding-pellet gap) with a linear heat source of value χ:

$$T_{ci} - T_{co} = \frac{1}{2\pi} \frac{\chi}{\lambda_{\text{clad}}(\overline{T}_{\text{clad}})} \ln\left(\frac{r_{co}}{r_{ci}}\right) \tag{2.56a}$$

$$T_{fs} - T_{ci} = \frac{1}{2\pi} \frac{\chi}{\lambda_{\text{gap}}(\overline{T}_{\text{gap}})} \ln\left(\frac{r_{ci}}{r_{fs}}\right) \tag{2.56b}$$

$$T_{fc} - T_{fs} = \frac{1}{4\pi} \frac{\chi}{\lambda_{\text{fuel}}(\overline{T}_{\text{fuel}})} \tag{2.56c}$$

Where the thermal conductivities λ_i are computed at the averaged temperatures of the fuel pellet, gap, and cladding. These expressions can then be used to verify that, at the point with the peak thermal power, the uranium dixoide fuel does not reach the melting temperature of $T_{\text{melt}} = 3120\ \text{K}$ during the postulated transient.

3 Computational solver structure

In the previous section, a set of design criteria and conditions has been introduced and a set of equations relating the various design parameters has been derived from these criteria. Next, the particular implementation of those equations that is used for this work, and its validity range, are exposed.

The overarching structure of the design algorithm consists of a feedback loop between three code modules. This feedback loop is iterated until a set of values is converged upon. These modules of the computational solver are:

- The *Core & Fuel Geometry Module* (GM), which computes the relevant geometric values of the reactor;
- The *Thermal-Hydraulics Module* (TM), which uses the dimensions from the GM to model the heat transfer from the fuel to the coolant in order to ensure that adequate cooling is maintained;
- The *Neutronics Module* (NM), which takes the inputs from the previous two modules and finds the enrichment level that makes such a configuration critical.

The steps in which the code obtains the optimal reactor design are next described in detail. Schematic summaries of the respective modules are shown in Figures 3.1 to 3.3.

3.1 Design Inputs

The computation begins with the user prescribing the five key input variables that the model uses to determine the rest of the design. These are:

- Reactor nominal thermal power $\dot{Q}_{nom}$
- Residual power fraction $\dot{Q}_{res}/\dot{Q}_{nom}$ to be removed by natural convection
- Coolant inlet temperature T_{in}
- Coolant inlet-outlet temperature difference ΔT
- Maximum permissible elevation for the dip-cooler H_{DC}

In addition to those, some of the model parameters may be modified by the user. These are:

- Maximum nominal coolant flow velocity, v_{nom}^{max}. By default, following [37], the maximum

coolant velocity is set at 2 m/s to prevent erosion of structural materials from the liquid lead

- Maximum allowed value for the fuel enrichment, e^{max}. Set by default at the regulated limit for civilian uses of 20%.
- Minimum Reynolds number for the natural convection flow, Re_{nat}^{min}
- Maximum value for the hoop stress in the cladding due to fission gas release, σ_h^{max}
- Burn-up of the fuel at EOL, $BU_{\%}$
- Maximum fraction of the core cross-section to be taken by the fuel, $\left(\frac{A_{\text{fuel}}}{A_{\text{core}}}\right)^{max}$
- The radial and axial peaking factors, F_R and F_Z

3.2 Preliminary calculations

The first values the model computes are the following:

- *Lead coolant properties*: density $\boldsymbol{\rho_{Pb}}$, dynamic viscosity $\boldsymbol{\mu_{Pb}}$, specific heat $\boldsymbol{c_p}$ and thermal conductivity $\boldsymbol{\lambda_{Pb}}$ (all correlations used within this work are detailed in Appendix A). These depend only on its temperature, and as it has been pointed out, the coolant at the core is assumed to be at the average temperature $T_{Pb} = T_{in} + \Delta T/2$, as consistent with the lumped parameters approach. The difference in coolant density between the inlet and outlet of the core $\boldsymbol{\Delta\rho_{Pb}}$, which depends only on the temperature difference $\boldsymbol{\Delta T}$ (given a linear density correlation), is also computed.
- *Initial guesses*. In addition to the user inputs and the values computed directly from those, for the first iteration the model requires values for the fuel temperature $\boldsymbol{T_{fuel}}$, total number of fuel rods in the core $\boldsymbol{N_{rod}}$, and coolant nominal velocity $\boldsymbol{v_{nom}}$ before new values can be subsequently computed and then be used in following iterative loops. Thus, the model takes the following initial values:
  - $T_f = 1200$ K
  - $N_{rod} = 222$, corresponding to 6 assemblies, each with 37 fuel pins (see Appendix B for details on how the number of fuel pins and fuel elements in a hexagonal lattice are obtained). For most of the input parameter values, this will prove to be too few rods, leading to excessive temperatures inside the fuel pellets; the model will adjust this value upwards accordingly as it goes through iterations.
  - $v_{nom} = v_{nom}^{max}$, as this value maximises the heat extracted from the core. The nominal velocity will be reduced iteratively if needed.
- The *nominal coolant pressure drop* $\boldsymbol{\Delta p_{nom}}$, which, as shown previously in Equation (2.34), can be computed directly from user inputs:

$$\Delta p_{nom} = g\,\Delta\rho_{Pb}\,H_{DC}\left(\frac{\dot{Q}_{res}}{\dot{Q}_{nom}}\right)^{b-2}$$

3.3 Core & Fuel Geometry Module

The relevant parameters regarding the geometry of the fuel pins and the core are computed next. Figure 3.1 summarizes the steps of which this module consists.

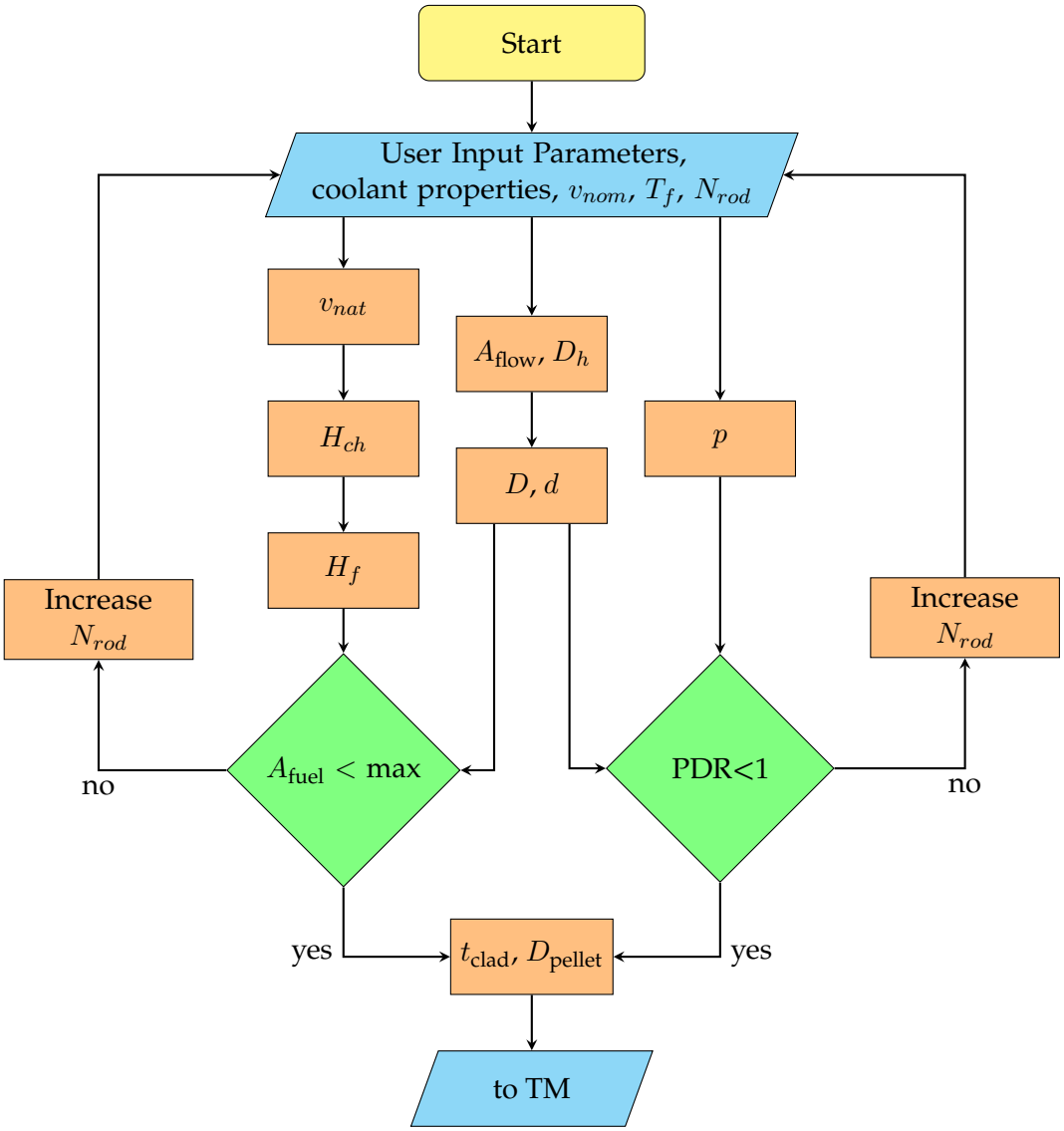

Figure 3.1: Structure of the Core and Fuel Geometry Module.

- The coolant natural circulation velocity v_{nat} is computed from the nominal velocity, according to Equation (2.33):

$$v_{nat} = \frac{\dot{Q}_{res}}{\dot{Q}_{nom}}\,v_{nom} \tag{3.1}$$

- Next, the height of the coolant channel H_{ch} is obtained by solving Equation (2.39) for this value:

$$H_{ch} = \mu_{Pb} \left(\mathrm{Re}_{nat}^{min}\right)^{1+b} \frac{2g\,\Delta\rho_{Pb}}{aK{\rho_{Pb}}^2} H_{DC} \frac{1}{{v_{nat}}^3} \tag{3.2}$$

- From that, as Equation (2.23) shows, the fuel height H_f is directly proportional to the channel height, and thus it can be computed as

$$H_f = H_{ch} \left(1 + \frac{R\,Y_{FG} BU_{\%}}{2\,M_{\mathrm{UO_2}}} \frac{\rho_f\,T_{FG}}{\mathrm{CTR}\,\sigma_h^{max}}\right)^{-1} \tag{3.3}$$

- The hydraulic diameter D_h and channel flow area A_{flow} are also obtained, using Equations (2.38) and (2.48), respectively:

$$D_h = \left(\frac{aK H_{ch}}{2g\,\Delta\rho_{Pb}(\Delta T)\,H_{DC}} {\rho_{Pb}}^{1-b}\,{v_{nat}}^{2-b}\,{\mu_{Pb}}^{b}\right)^{1/1+b}$$

$$A_{\mathrm{flow}} = \frac{F_R\,\dot{Q}_{nom}}{2\,N_{rod}\,\rho_{Pb}\,v_{nom}\,c_p\,\Delta T}$$

- From those, the diameters of the fuel rod, D, and the spacer wire, d, are computed, following (2.44):

$$D = \frac{4}{\pi}\left[\frac{A_{\mathrm{flow}}}{D_h} + \sqrt{\left(\frac{A_{\mathrm{flow}}}{D_h}\right)^2\left(\frac{4\sqrt{3}}{\pi} - 1\right) - \frac{\pi}{4}A_{\mathrm{flow}}}\right]$$

$$d = \frac{4}{\pi}\left[\frac{A_{\mathrm{flow}}}{D_h} - \sqrt{\left(\frac{A_{\mathrm{flow}}}{D_h}\right)^2\left(\frac{4\sqrt{3}}{\pi} - 1\right) - \frac{\pi}{4}A_{\mathrm{flow}}}\right]$$

  It is important to note that those can only be computed if the square root can be obtained, i.e. if the *discriminant* is positive. It can be shown that this value grows if the nominal coolant velocity v_{nom} is decreased (since doing this both increases A_{flow} and decreases D_h). Therefore, if the square root can not be obtained, the value of v_{nom} is slightly reduced and the module is computed again.

- Separately, the pitch p can be obtained from the inputs, as shown in Equation (2.51):

$$p = \frac{4}{\pi}\frac{F_R\,\dot{Q}_{nom}}{N_{rod}\,c_p\,\Delta T}\frac{1}{\mu_{Pb}\,Re_{nat}^{min}}\left(\frac{\dot{Q}_{res}}{\dot{Q}_{nom}}\right)$$

- At this point, the values for the diameters and the pitch obtained in the previous steps are checked for consistency:

  – *Total fuel cross-section*. Using the number of fuel rods, N_{rod}, and their diameter, D, the fraction of the core cross-section area occupied by the fuel pins, obtained in Equation (2.3), is checked to be below the prescribed maximum:

$$\frac{A_{\text{fuel}}}{A_{\text{core}}} = \frac{D^2 N_{rod}}{{H_f}^2} < \left(\frac{A_{\text{fuel}}}{A_{\text{core}}}\right)^{max} \tag{3.4}$$

  – *Pitch-to-diameter ratio*. Separately, the value of D must be, by construction, lower than the pitch p, i.e. the *pitch-to-diameter ratio*, or PDR, must be larger than unity:

$$\text{PDR} = \frac{p}{D} > 1 \tag{3.5}$$

  (note that this is equivalent to stating that $d > 0$). If either of this conditions is not met, the number of rods is increased and the computation is carried out again.

- Finally, the remaining parameters regarding the fuel rod are computed.

  – The cladding thickness, t_{clad}, is obtained using the cladding thickness ratio exposed in Equation (2.11):

$$t_{\text{clad}} = CTR \cdot D \tag{3.6}$$

  – The diameter of the fuel pellet, D_{pellet}, is therefore computed as

$$D_{\text{pellet}} = D - 2\,t_{\text{clad}} - 2\,t_{\text{gap}} \tag{3.7}$$

  Where, in addition to previously calculated values, it has been used that the gap thickness is set as $t_{\text{gap}} = 0.1$ **mm** and the aforementioned cladding thickness ratio, or ratio between the thickness and the average diameter of the cladding, is taken as $\text{CTR} = 0.05$[1].

3.4 Thermal-Hydraulics Module

Once a fuel geometry has been output by the GM, the heat transfer in that core is modelled, in order to evaluate whether sufficient cooling is achieved. Figure 3.2 displays the steps in this module, which are exposed next.

[1] For the scope of this work, the number of degrees of freedom regarding fuel rod geometry must be constrained, in order for the feedback loop between fuel rod size and fuel centerline temperature to be manageably simple. Furthermore, optimizing values such as the cladding-pellet gap would involve other factors other than heat transmission, such as neutron economy and material fuel-cladding interaction. Thus, the cladding thickness ratio and gap thickness are fixed at usual values for the present kind of reactor, so that a single variable describes the geometry completely.

- *Linear power*. With the current guess for the number of fuel rods N_{rod}, and with the fuelled core height H_f from the GM, the average linear power of the reactor is computed, as per Equation (2.52):

$$\overline{\chi} = \frac{\dot{Q}_{nom}}{N_{rod}\, H_f}$$

  As well as the linear power for the peak assembly during a power doubling transient, as shown in Equation (2.54):

$$\chi_{\text{peak}} = 2\, F_R\, F_Z\, \overline{\chi}$$

- *Coolant flow parameters*. The values from the GM are used to obtain the Nusselt number $\mathbf{Nu}_{Pb}$, which depends on the flow velocity, pitch-to-diameter ratio and hydraulic diameter. The Nusselt number reflects the ratio of convection and conduction as heat transfer mechanisms across a solid-fluid boundary. In this work, it is computed using the following correlation:

$$\mathbf{Nu} = 0.047 \left(1 - \mathbf{e}^{-3.8(\text{PDR}-1)}\right) \left(\mathbf{Pe}^{0.77} + 250\right) \tag{3.8}$$

  With the Péclet number **Pe** computed itself from other two fluid dynamics adimensional parameters, the Reynolds number **Re** and the Prandtl number **Pr**:

$$\mathbf{Pe} = \mathbf{Re} \cdot \mathbf{Pr} = \frac{\rho\, v\, D_h\, c_p}{\lambda} \tag{3.9}$$

- *Temperature*. At this point, the temperature profile of the peak fuel rod during a power doubling transient can be obtained. To do so, the steps are the following, where $\chi = \chi_{\text{peak}}$ is taken:

  - First, the temperature difference between the outer surface of the cladding and the average coolant temperature can be obtained directly, as expressed in Equation (2.55):

$$T_{co} - T_{Pb} = \frac{D_h}{\pi D} \frac{\chi}{\lambda_{Pb}(T_{Pb})\, \mathbf{Nu}_{Pb}} \tag{3.10}$$

  - Once the outer cladding temperature T_{co} is known, the remaining temperatures at the inner surface of the cladding T_{ci}, the outer surface of the pellet T_{fs} and the centerline of the fuel T_{fc} can be successively obtained. However, as the equations (2.56) show, the conductivities λ_i are dependent on the temperatures themselves, which are unkown a priori.

    The way this is approached here is to first compute an approximation of the conductivity, which is used to estimate the new temperature, and which then can be used

to refine the estimate for λ_i, allowing for the process to be iterated until the values converge. Taking, for instance, the calculation of the temperature difference across the cladding, the thermal conductivity is first estimated using the (known) cladding outer temperature T_{co}:

$$\lambda_{\text{clad}}^{(0)} = \lambda_{\text{clad}}(T_{co}) \tag{3.11}$$

With the superindex $^{(0)}$ indicating that it corresponds to the first iteration. Then, this estimate is used to approximate the temperature at the inner cladding surface, following Equation (2.56a):

$$T_{ci}^{(0)} = T_{co} + \frac{1}{2\pi}\frac{\chi}{\lambda_{\text{clad}}^{(0)}} \ln\left(\frac{r_{co}}{r_{ci}}\right) \tag{3.12}$$

At this point, the conductivity estimate can be refined by evaluating the corresponding function at the average of the outer and inner temperatures:

$$\lambda_{\text{clad}}^{(1)} = \lambda_{\text{clad}}\left(\frac{T_{co} + T_{ci}^{(0)}}{2}\right) \tag{3.13}$$

This closer approximation of the value of $\lambda_{\text{clad}}(\overline{T}_{\text{clad}})$ will yield a better estimate for T_{ci}, which is then used to refine the value of the conductivity, and so forth. The process is found to converge in only a few iterations, thus carrying a relatively low computational cost. The rest of the temperatures are then obtained using a completely analogous process.

- Once the peak temperature of the fuel during the power doubling transient, ${T_{fc}}^*$, is obtained, its value is compared to the melting temperature T_{melt}:
  - If ${T_{fc}}^* > T_{\text{melt}}$, then the current value of N_{rod} is not consistent with a core that can sustain a power doubling transient without having the fuel reach the melting point. Then, the value of N_{rod} is increased to the next geometrically valid configuration, and used as an input for the next iteration of the GM.
  - On the other hand, if ${T_{fc}}^* < T_{\text{melt}}$, a valid configuration has been found and the algorithm goes to the next step.
- *Fuel temperature update*. Finally, one must recall that at the beginning of the process, a fuel temperature estimate of $T_f = 1200$ K was taken. This value is used to compute the fuel density, relevant for the pitch-to-diameter ratio and the gas plenum volume. Upon successful calculation of a valid core geometry that leads to sufficient cooling, a more accurate fuel temperature estimate is used instead of that initial guess in the next iteration.

  To this end, the nominal fuel temperature profile is computed in the same way as previously, but taking the nominal average linear power instead, i.e. $\chi = \overline{\chi}$, and hence obtaining the fuel pellet temperature. With this updated value, the algorithm starts over at the GM.

It is found that this adjustment of the fuel density via its temperature has a modest effect on the overall results, but given that it rarely takes the code more than a handful of iterations for this value to converge, and thus has a low computational cost, it is still pursued.

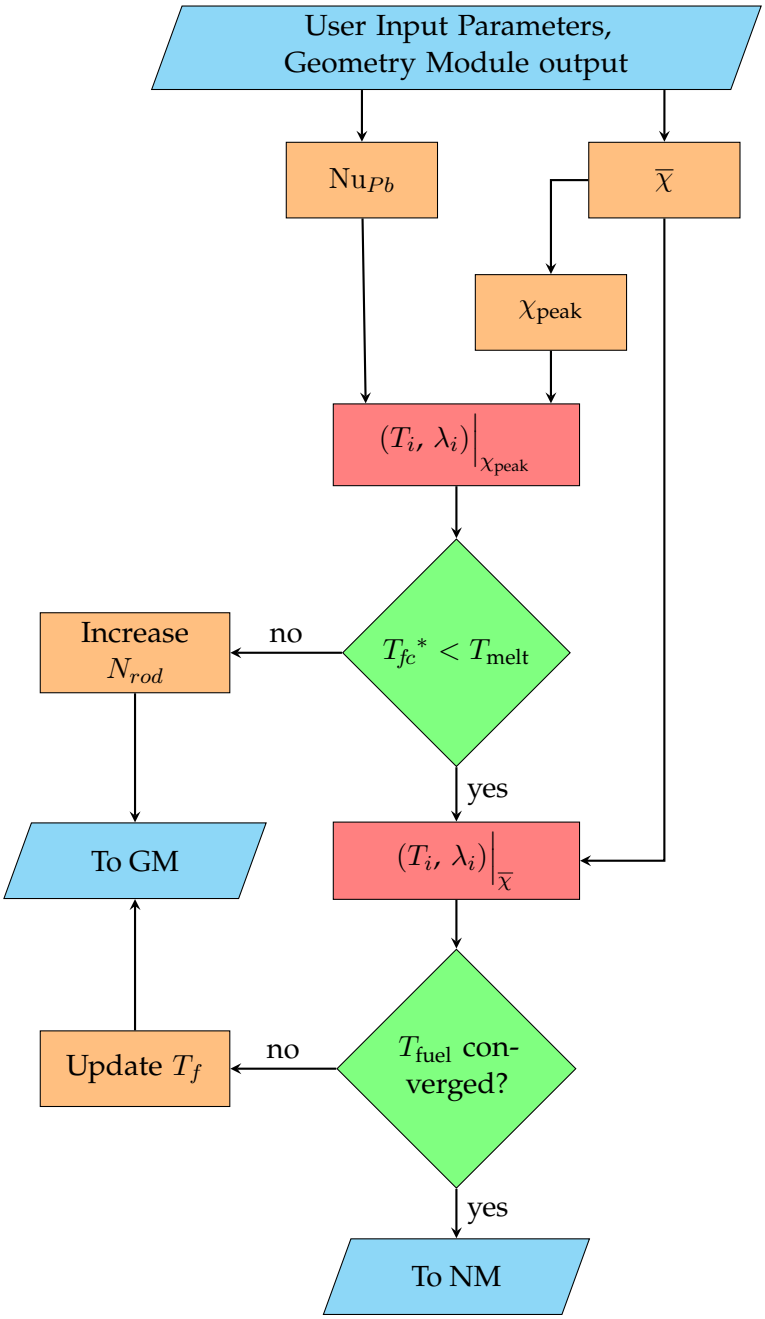

Figure 3.2: Structure of the Thermal-Hydraulics Module.

3.5 Neutronics Module

Once this point is reached, a core geometry capable of passive cooling and consistent with the required parameters has been found. The last step is to obtain and enrichment value such that this configuration is critical. This is done in an iterative manner as well, outlined next.

- *Initial guess*. The value of the enrichment is set at $e = e^{(0)} = 0.01$ in order to be able to obtain a value for the multiplication factor k.

- *Buckling, atom densities, cross-sections, diffusion coefficient*. The buckling can be first obtained from the core dimensions, as shown in Equation (2.5). Separately, with the current value of e, and using the geometrical parameters of the core from previous sections, the number densities of ^{235}U, ^{238}U and Fe are obtained, following Equations (2.8) to (2.10). From those, the macroscopic fission, capture and absorption cross-sections can be obtained, and subsequently the diffusion coefficient is computed (Equations (2.12) to (2.15)).

$$B^2 = \left(\frac{2.405}{\tilde{R}}\right)^2 + \left(\frac{\pi}{\tilde{Z}}\right)^2 \; ; \quad \tilde{H} = \frac{3}{2} H_f \; ; \qquad \tilde{R} = \frac{3}{4} H_f$$

$$\begin{aligned} N^{235} &= e \, \frac{\rho_f N_A}{M_{UO_2}} \frac{D^2_{\text{pellet}} \, N_{rod}}{{H_f}^2} \\ N^{238} &= (1 - e) \, \frac{\rho_f N_A}{M_{UO_2}} \frac{D^2_{\text{pellet}} \, N_{rod}}{{H_f}^2} \\ N^{\text{clad}} &= \frac{\rho_{\text{clad}} \, N_A}{M_{\text{clad}}} \, \text{CTR}(2 - \text{CTR}) \, \frac{D \, N_{rod}}{{H_f}^2} \end{aligned}$$

$$\begin{aligned} \Sigma_f &= N^{235} \sigma_f^{235} + N^{238} \sigma_f^{238} \\ \Sigma_c &= = N^{235} \sigma_c^{235} + N^{238} \sigma_c^{238} + N^{\text{clad}} \sigma_c^{\text{clad}} \\ \Sigma_a &= \Sigma_f + \Sigma_c \end{aligned}$$

$$D = \Sigma_a \, L^2$$

- *Multiplication factor*. Using the values from the previous step, the multiplication factor k is obtained as shown in Equation (2.7):

$$k = \frac{\nu \Sigma_f}{D B^2 + \Sigma_a} \tag{3.14}$$

- *Adjust enrichment*. At this point, either

  - $k = 1.0$. An enrichment value that makes this core configuration critical has been found (symbolised as e^*), and the code proceeds to the next step.

  - $k \neq 1.0$. The enrichment value is adjusted by computing the next iteration as

$$e^{(i+1)} = \frac{1}{k} e^{(i)}$$

So that if $k > 1.0$, i.e. the reactor is supercritical, the enrichment is lowered, and if on the other case $k < 1.0$, i.e. subcritical, e is increased. This value is then used to compute the parameters again, until the proper value is converged upon.

- *Check enrichment is valid*. The last step in the algorithm is to compare the critical value of e^* just obtained with the user-provided maximum allowed enrichment, e^{max}.
  - If $e^* \leq e^{max}$, the computation is finished and the code outputs the results.
  - If, on the other hand, $e^* > e^{max}$, this means no valid configuration has been found. The procedure in this case is to decrease the coolant nominal flow velocity[2], v_{nom}, which was initially set at the maximum value of v_{nom}^{max}. With this new value, the algorithm is initialised again, at the GM, and a new solution is found.

The steps in the NM can be visualized in Figure 3.3.

[2]It is found empirically that increasing N_{rod} at this point and looping back to the TM does not produce a lower enrichment, i.e. for a given (p, H_f), increasing N_{rod} (and therefore decreasing D_{pellet}) results in a slightly lower, not higher, fuel mass; so that the enrichment must increase to compensate. On the other hand, slightly decreasing v_{nom} increases H_f (which is proportional to v_{nom}^{-3}, see Equations (3.2) and (3.3)); subsequently increasing the overall fuel mass and therefore allowing for a lower enrichment.

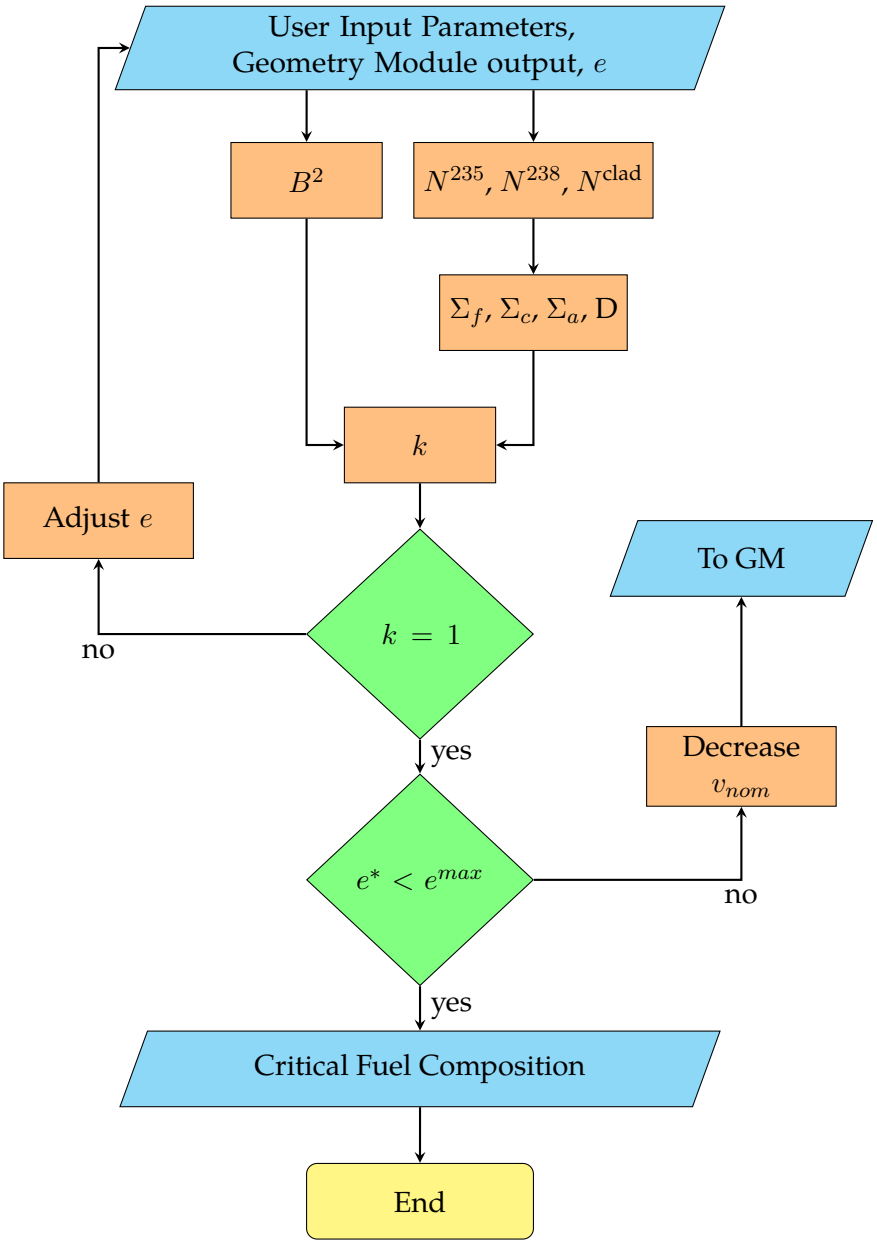

Figure 3.3: Structure of the Neutronics Module.

4 Analysis and conclusions

All models are wrong, but some are useful.
— British statistician George Box (1976)

4.1 The *ADELE* application

As the analytical algorithm of *ADELE* is implemented as an application for mobile platforms, an integral part of this project involves the building of the application itself, i.e. the development of a simple graphical interface for parameter input and visualization.

This application is built using the SwiftUI[32] programming language, the native language specifically produced for software development on Apple operating systems. The app will be made available from the Apple App Store for iPhone and iPad devices. Among the intended users of the system are the Nuclear Engineering students, so that they may have a simple tool to develop an intuitive understanding of the effect of the various parameters in the design of the core.

The app features, after a welcome screen, a *view* for the input of the reactor parameters. This screen features appropriately labelled sliders so that the user may modify the default values for any of these inputs. Some preset parameter values, corresponding to specific LFR designs, are also available.

Upon the computing of the reactor parameters, the screen changes to a list of those output values. If, for some reason, the computation returns an error (in case, for instance, that the combination of input parameters causes the algorithm to not converge upon a design), a pop-up alert appears instead, informing the user, and the view returns to the input parameters screen.

Additionally, a view of the core cross-section is available from the computed parameters view. It schematically shows the number of hexagonal fuel assemblies that the algorithm has found as a solution, arranged in their hexagonal grid and featuring the fuel pins. Of course, this view is for illustrative purposes only, since *i*) the algorithm does not consider the different fuel assemblies, but only the total number of rods; the number of assemblies and the fuel pins in each assembly is merely chosen in order to fit the required total number of rods, and *ii*) *ADELE* does not consider the effects of control assemblies or any other heterogeneous feature (other than the effect of the empty space for the middle assembly on the radial peaking factor).

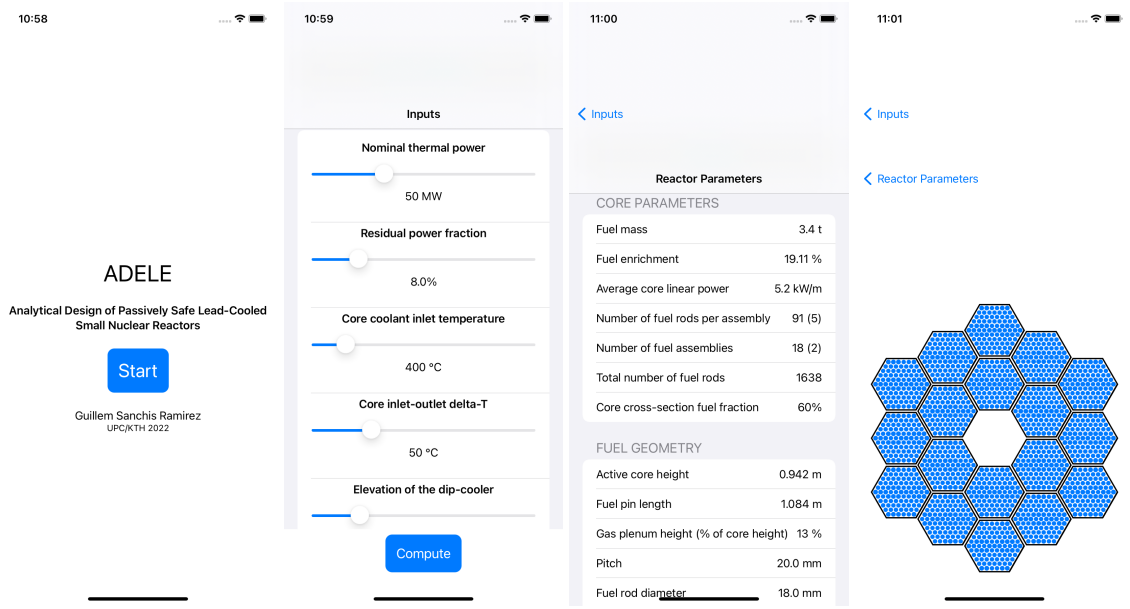

Figure 4.1: The various views featured in the *ADELE* core design mobile application.

4.2 Benchmarking. SUNRISE-LFR and SEALER-Arctic

As a way to verify the proposed analytical approach, the outputs of *ADELE* are first compared to the parameters for the SUNRISE-LFR reactor given by F. Dehlin[34]. This is useful because some of the assumptions followed in the referred work are also used here, namely a fundamental-physics based, condensed parameters approach built around the establishing of natural convection cooling of residual heat; while at the same time using separate tools, like iterated Monte Carlo simulations, in the design process. It provides therefore a good starting point of comparison for *ADELE*.

The parameters that must be given as an input are therefore obtained from [34] and are shown in Table 4.1. Those are used as an input to obtain the parameters of SUNRISE-LFR; they arise from either materials considerations, or supported by Monte Carlo simulations as a part of the design process.

Parameter (units)	**Value**
Nominal Thermal Power (MW)	80
Residual Power Fraction (%)	12.5
Core coolant inlet temperature (°C)	420
Core inlet-oulet ΔT (°C)	130
Elevation of the dip-cooler (m)	3.50
Maximum coolant nominal velocity (m/s)	1.5
Radial peaking factor	1.51
Axial peaking factor	1.21

Table 4.1: Main input parameters for the SUNRISE-LFR case[34]. Note that the peaking factors are different that the ones mentioned throughout this work; the ones from the reference are obtained partially using Monte Carlo methods and are used as inputs for *ADELE*.

The output parameters of *ADELE* for these inputs are then compared to the ones from the SUNRISE-LFR reactor. The main ones are listed in Table 4.2 below.

Parameter (units)	**SUNRISE-LFR**	***ADELE***
Fuel enrichment (%) †	12.0	11.8
Number of fuel rods	11718	12810
Average linear power (kW/m)	6.21	4.8
Fuel column height (m)	1.010	1.292
Fuel pin length (m)	1.750	1.518
Fuel assembly pitch (mm)	13.0	11.9
Fuel rod diameter (mm)	11.8	10.6
PDR	1.10	1.12
Fuel pellet diameter	10.0	9.4
Spacer wire diameter (mm)	1.2	1.2

Table 4.2: Reactor parameters of SUNRISE-LFR and output values generated with *ADELE* using the same inputs. (†) The fuel considered in [34] is uranium nitride (UN), with a different atom density to the UO_2 assumed in *ADELE*. Therefore the neutronics are not directly comparable. However, the fuel enrichment value is provided for reference.

Some of the design parameters of SUNRISE-LFR are obtained following a similar analytical approach as in *ADELE* and therefore it is not surprising that the yielded results are similar; it nevertheless serves as a useful validation of the algorithm. Others, however, are obtained independently, and therefore are a good metric for the accuracy of the analytical approach presented here.

This is the case, for instance, of the fuel column height. In the case of the SUNRISE-LFR core it is obtained using the Monte Carlo code Serpent2, after independently postulating a coolant channel length as an input to the design process. While there is a discrepancy between the values for this height using both methods, one must bear in mind that the value in *ADELE* is arrived at entirely without any consideration of the core structure in the neutronics calculations, but rather assuming the simple case of a homogeneous reflected reactor and only one energy group. Indeed, it is fair to point out that the fuel pin length is postulated *a priori* in the design of SUNRISE-LFR, while it is arrived to analytically in *ADELE*. Since this value is directly proportional to the fuelled height, which in turn inversely correlates to the linear power value, part of the discrepancy in those two parameters may be due simply to the intial chosen value for the rod length in SUNRISE-LFR.

Also remarkable is the agreement in the total number of fuel pins; more so because in [34] this value is a set input postulated in order to carry out the design, while, again, it is an analytically computed value in the case of *ADELE*.

Thus, *ADELE* reproduces the SUNRISE-LFR parameters with an accuracy that is quite good given the much lower computational load it requires to obtain them.

As a second set of verification parameters, the characteristics of the SEALER-Arctic[30], designed by LeadCold, are reproduced. The relevant reactor parameters are obtained from [18] and are listed on Table 4.3. SEALER-Arctic is a smaller reactor, which means the peaking factors are accordingly higher; while the design core temperatures are lower in order to limit the material

corrosion in the core to a point that the system can serve for several years in remote locations.

Parameter (units)	Value
Nominal Thermal Power (MW)	8
Residual Power Fraction (%)	10.0
Core coolant inlet temperature (°C)	390
Core inlet-oulet ΔT (°C)	42
Elevation of the dip-cooler (m)	2.2
Maximum coolant nominal velocity (m/s)	1.5
Radial peaking factor	1.55
Axial peaking factor	1.41

Table 4.3: Main reactor parameters of SEALER-Arctic, gathered from [18]. Peaking factors are obtained in the reference from Monte Carlo analysis; those values are used as inputs for the analytical method.

As in the previous case, the maximum coolant velocity is observed, after the design is fixed, to be around 1.5 m/s. Therefore, this is the value used as an input for the maximum allowed coolant velocity for *ADELE*, in order to reproduce the reactor parameters. With those values as inputs, the analytical algorithm produces the core design whose main parameters are displayed in Table 4.4.

Parameter (units)	SEALER-Arctic	*ADELE*
Fuel mass (t)	2.5	3.4
Fuel enrichment (%)	19.75	19.11
Number of fuel rods	1729	1638
Average linear power (kW/m)	4.2	5.2
Fuel column height (m)	1.105	0.942
Fuel pin length (m)	1.590	1.084
Fuel assembly pitch (mm)	16.4	20.0
Fuel rod diameter (mm)	14.5	18.0
PDR	1.127	1.115
Fuel pellet diameter	13.4	16.0
Spacer wire diameter (mm)	1.8	2.1

Table 4.4: Reactor parameters of SEALER-Arctic, obtained from [18] and reproduced analytically using *ADELE*.

The design of SEALER-Arctic in [18] is obtained with a conjunction of a multi-variable fast reactor design code (see [36]) coupled with the Monte Carlo code Serpent, in a similar way as in the previous case. Once more, then, the agreement between those values and the outputs of *ADELE* is quite remarkable, considering the simplicity of the analytical model.

In a similar way as with SUNRISE-LFR, *ADELE* seems to underestimate the fuel column and fuel pin lengths. For the case of the fuel length, it is hypothesised that the assumption that the homogeneous model of the core to have its height equal to its diameter may not give the code enough flexibility to find a more optimal design. It is, however, a useful simplification since it allows for a more straightforward derivation. A refining in that aspect, then, may be a good

further work for the model. As for the ratio between the fuel and pin lengths, which corresponds to the fission gas plenum, it is possible that the discrepancy is due to the difficulty of precisely estimating the fuel burn-up at BOL in a range of designs.

4.3 Conclusions

A design code for lead-cooled fast neutron nuclear reactors has been developed. This code takes advantage of a lumped parameters approach in order to obtain the main reactor parameters from fundamental physics using exclusively algebraic equations. It therefore features a very low computational load when compared to the standard procedure based on iterative Monte Carlo simulations. Despite the obvious drawback in the loss of precision stemming from the simplifications that are taken, the resulting reactor parameters are reasonably accurate. This allows for very rapid iteration with different input values, allowing for the quick exploration of a broad design space when first considering such a system.

The analytical algorithm is implemented in the *ADELE* mobile application. The low computational load of the system allows it to run in such computing devices without being constrained by the hardware. This application can be a valuable tool e.g. for Nuclear Engineering students, since it can help develop an intuition for the different factors affecting the design of an LFR in particular, and a nuclear reactor in general.

Regarding future work, some potential courses are identified. In terms of improving the analytical model, the modelling of the core as a homogeneous system may be refined. On the one hand, the core geometry may be expanded by allowing a range of ratios between the diameter and the active height, and the core volume calculation may be made more precise by taking hexagonal assemblies into account instead of a straight cylinder. Also, it is likely that the modelling of the neutron flux using more energy groups would improve the accuracy of the criticality calculations without a prohibitive increase in computational cost. Furthermore, solving the flux in a fully reflected cylindrical geometry would yield a more exact characterization, e.g. for the buckling. Separately, developing the numerical implementation of differential equations in SwiftUI would open the door to the simulation of various postulated transients, in turn refining the analytical parameters. Finally, developing the *ADELE* application for other computational systems, namely Android, would make it more accessible to potential users.

Acknowledgements

To Professor Janne Wallenius, for your constant support and advice before, during and after my internship at KTH. I thoroughly enjoyed my time working with you, and your feedback throughout this work has been invaluable.

Furthermore, to the Nuclear Engineering division and the rest of the Physics Department of KTH. It has provided a stimulating and exciting working environment, and the relationships with the faculty and students will be cherished for ever. In particular, to Alessandro Persico, Guan Wang, Fredrik Dehlin, and Ibrahim Batayneh for all the conversations. I wish you all the best.

Also to Marc Altés, Andrea Serrano, and the rest of my colleagues at the MUEN, and to Professor Lluís Batet and all the other professors from the Master's program. I am sure we will meet again in the future.

Finally, my sincerest gratitude to my parents, Eduard and María José, without whom this would not have been possible; and to my girlfriend, Maria, for her unconditional support. Thank you all.

Bibliography

[1] Our World in Data. *The world's energy problem*. URL: https://ourworldindata.org/grapher/consumption-co2-per-capita-vs-gdppc. (accessed: February 14th, 2022).

[2] Our World in Data. *What are the safest and cleanest sources of energy?* URL: https://ourworldindata.org/safest-sources-of-energy. (accessed: February 14th, 2022).

[3] Nuclear Energy Agency. *Projected Costs of Generating Electricity*. https://www.oecd-nea.org/jcms/pl_51110/projected-costs-of-generating-electricity-2020-edition?id=pl_51110&preview=true. 2020. (accessed: February 14th, 2022).

[4] J.R. Lovering, A. Yip, and T. Nordhaus. "Historical construction costs of global nuclear power reactors". In: *Energy Policy* **91** (2016), pp. 371–382. DOI: https://doi.org/10.1016/j.enpol.2016.01.011.

[5] *The World Nuclear Industry Status Report 2012*. https://www.worldnuclearreport.org/-World-Nuclear-Industry-Status-Report-2012-.html. 2012.

[6] US Department of Energy. "DOE Invests $61 Million in Advanced Nuclear Energy R&D Projects Across America". In: *energy.gov* (June 22, 2021). URL: https://www.energy.gov/articles/doe-invests-61-million-advanced-nuclear-energy-rd-projects-across-america (visited on 02/15/2022).

[7] "Nuclear and gas criteria set for inclusion in EU taxonomy". In: *World Nuclear News* (Jan. 6, 2022). URL: https://www.world-nuclear-news.org/Articles/Nuclear-and-gas-criteria-set-for-inclusion-in-EU-t (visited on 02/15/2022).

[8] "China's Climate Goals Hinge on a $440 Billion Nuclear Buildout". In: *Bloomberg* (Nov. 2, 2021). URL: https://www.bloomberg.com/news/features/2021-11-02/china-climate-goals-hinge-on-440-billion-nuclear-power-plan-to-rival-u-s (visited on 02/15/2022).

[9] Associated Press. "Coal-dependent West Virginia eliminates ban on nuclear power". In: *NPR* (Feb. 8, 2022). URL: https://www.npr.org/2022/02/08/1079339405/west-virginia-ban-nuclear-power-coal?t=1644928161601 (visited on 02/15/2022).

[10] World Energy Council. *The Future of Nuclear: Diverse Harmonies In the Energy Transition*. https://www.worldenergy.org/publications/entry/world-energy-scenarios-2019-the-future-of-nuclear-diverse-harmonies-in-the-energy-transition. 2019. (accessed: February 14th, 2022).

[11] D. Ruzik. *Economics of Nuclear Reactor*. https://www.youtube.com/watch?v=cbeJIwF1pVY. 2019. (accessed: February 15th, 2022).

[12] World Nuclear. *Nuclear Power Economics and Project Structuring*. https://world-nuclear.org/our-association/publications/online-reports/nuclear-power-economics-and-project-structuring.aspx. 2017. (accessed: February 15th, 2022).

[13] International Atomic Energy Agency. *Small modular reactors*. https://www.iaea.org/topics/small-modular-reactors. (accessed: February 15th, 2022).

[14] *Generation IV International Forum*. https://www.gen-4.org/gif/. (accessed: February 15th, 2022).

[15] Generation IV International Forum. *Generation IV Systems*. https://www.gen-4.org/gif/jcms/c_59461/generation-iv-systems. (accessed: February 15th, 2022).
[16] J. Wallenius and S. Bortot. *Fast neutron Generation IV reactors*. Publisher?
[17] World Nuclear Association. *Fast Neutron Reactors*. https://world-nuclear.org/information-library/current-and-future-generation/fast-neutron-reactors.aspx. 2021. (accessed: February 15th, 2022).
[18] Janne Wallenius et al. "Design of SEALER, a very small lead-cooled reactor for commercial power production in off-grid applications". In: *Nuclear Engineering and Design* **338** (2018), pp. 23–33. DOI: https://doi.org/10.1016/j.nucengdes.2018.07.031.
[19] Concetta Fazio. *Handbook on Lead-bismuth Eutectic Alloy and Lead Properties, Materials Compatibility, Thermalhydraulics and Technologies*. OECD-NEA, 2015.
[20] B.F. Gromov *et al.* "Use of lead-bismuth coolant in nuclear reactors and accelerator-driven systems". In: *Nuclear Engineering and Design* **173** (1997), pp. 207–217. DOI: https://doi.org/10.1016/S0029-5493(97)00110-6.
[21] Jesper Ejenstam emphet al. "Oxidation studies of Fe10CrAl–RE alloys exposed to Pb at 550 °C for 10,000 h". In: *Journal of Nuclear Materials* **443** (2013), pp. 161–170. DOI: https://doi.org/10.1016/j.jnucmat.2013.07.023.
[22] Jesper Ejenstam and Peter Szakálos. "Long term corrosion resistance of alumina forming austenitic stainless steels in liquid lead". In: *Journal of Nuclear Materials* **461** (2015), pp. 164–170. DOI: https://doi.org/10.1016/j.jnucmat.2015.03.011.
[23] Peter Dömstedt, Mats Lundberg, and Peter Szakálos. "Corrosion Studies of Low-Alloyed FeCrAl Steels in Liquid Lead at 750 °C". In: *Oxidation of Metals* **91** (2019), pp. 511–524. DOI: https://doi.org/10.1007/s11085-019-09896-z.
[24] Peter Dömstedt, Mats Lundberg, and Peter Szakálos. "Corrosion studies of a low alloyed Fe–10Cr–4Al steel exposed in liquid Pb at very high temperatures". In: *Journal of Nuclear Materials* **531** (2020). DOI: https://doi.org/10.1016/j.jnucmat.2020.152022.
[25] *SUNRISE*. https://www.reactor.sci.kth.se/sunrise/sunrise-1.999712. (accessed: April 2022).
[26] Swedish Foundation for Strategic Research (SSF). *SSF Agenda 2030 Research Centers*. https://strategiska.se/en/apply-to-ssf-agenda-2030-research-centers-arc-on-future-advanced-technology-for-sustainabilty/. (published: August 26th, 2019; accessed: April 2022).
[27] *SEK 99 million to small lead-cooled nuclear reactors*. https://www.kth.se/en/om/nyheter/centrala-nyheter/99-miljoner-till-sma-blykylda-karnreaktorer-1.1141788. (published: February 21st, 2022; accessed: April 2022).
[28] *SUNRISE - Work Plan*. https://www.reactor.sci.kth.se/sunrise/sunrise-work-plan-1.999730. (accessed: April 2022).
[29] *LeadCold - Atomic Simplicity*. https://www.leadcold.com/about-us.html. (accessed: April 2022).
[30] *SEALER design*. https://www.leadcold.com/sealer.html. (accessed: April 2022).
[31] Sara Bortot, Erdenechimeg Suvdantsetseg, and Janne Wallenius. "BELLA: a multi-point dynamics code for safety-informed design of fast reactors". In: *Annals of Nuclear Energy* **85** (2015), pp. 228–235. DOI: https://doi.org/10.1016/j.anucene.2015.05.017.
[32] Apple. *SwiftUI Overview*. https://developer.apple.com/xcode/swiftui/. (accessed: April 2022).
[33] John R. Lamarsh and Anthony J. Baratta. *Introduction to Nuclear Engineering (Third Edition)*. Pearson, 2001.

[34] Fredrik Dehlin, Janne Wallenius, and Sara Bortot. "An analytic approach to the design of passively safe lead-cooled reactors". In: *Annals of Nuclear Energy* **169** (2022). DOI: https://doi.org/10.1016/j.anucene.2022.108971.

[35] S. K. Chen, Y. M. Chen, and N.E. Todreas. "The upgraded Cheng and Todreas correlation for pressure drop in hexagonal wire-wrapped rod bundles". In: *Nuclear Engineering and Design* **335** (2018), pp. 356–373. DOI: https://doi.org/10.1016/j.nucengdes.2018.05.010.

[36] Staffan Qvist and Ehud Greenspan. "The ADOPT code for automated fast reactor core design". In: *Annals of Nuclear Energy* **71** (2014), pp. 23–36. DOI: https://doi.org/10.1016/j.anucene.2014.03.013.

[37] A. *et al.* Weisenburger. *Materials for ALFRED and ELFR selection and challenges*. IAEA, 2015.

[38] Juan J. Carbajo *et al.* "A review of the thermophysical properties of MOX and UO_2 fuels". In: *Journal of Nuclear Materials* **299** (2001), pp. 181–198. DOI: https://doi.org/10.1016/S0022-3115(01)00692-4.

[39] Aritra Banerjee *et al.* "Thermal property characterization of a titanium modified austenitic stainless steel (alloy D9)". In: *Journal of Nuclear Materials* **347** (2005), pp. 20–30. DOI: https://doi.org/10.1016/j.jnucmat.2005.06.009.

[40] L. Leibowitz and R.A. Blomquist. "Thermal conductivity and thermal expansion of stainless steels D9 and HT9". In: *International Journal of Thermophysics* **9** (1988), pp. 873–883. DOI: https://doi.org/10.1007/BF00503252.

Appendix A Correlations

Uranium oxide properties

The correlations used for the density and thermal conductivity of the fuel are obtained from [38] and are listed next:

$$\rho_{UO_2}(T) = 10970\left(0.99734 + 9.802\cdot 10^{-6}\,T - 2.705\cdot 10^{-10}\,T^2 + 4.391\cdot 10^{-13}\,T^3\right) \quad \left[\mathrm{kg\,m^{-3}}\right]$$

$$\lambda_{UO_2}(T,p) = 1.158\left(\frac{100}{7.5408 + 17.692\frac{T}{1000} + 3.6142\left(\frac{T}{1000}\right)^2} + \right.$$
$$\left. + \frac{6400}{\left(\frac{T}{1000}\right)^{5/2}}\exp\left(-\frac{16.35}{T/1000}\right)\right)\left(\frac{1-p}{1+2p}\right) \quad \left[\mathrm{W\,m^{-1}\,K^{-1}}\right]$$

Where in this case p is the porosity of the fuel pellet (fixed for this work at 5%).

Lead coolant properties

The density, thermal conductivity, specific heat and dynamic viscosity of liquid lead are obtained from [18]:

$$\rho_{Pb}(T) = 11321 - 1.222\,T \quad \left[\mathrm{kg\,m^{-3}}\right]$$
$$\lambda_{Pb}(T) = 10.5 + 0.0075\,T \quad \left[\mathrm{W\,m^{-1}\,K^{-1}}\right]$$
$$c_p(T) = -1.524\cdot 10^6\frac{1}{T^2} + 176.2 - 4.923\cdot 10^{-2}\,T + 1.544\cdot 10^{-5}\,T^2 \quad \left[\mathrm{J\,kg^{-1}\,K^{-1}}\right]$$
$$\mu_{Pb}(T) = 4.55\cdot 10^{-4}\,\mathrm{e}^{\frac{1069}{T}} \quad \left[\mathrm{Pa\,s^{-1}}\right]$$

Cladding and gap properties

For the density and conductivity of the cladding, data pertaining to the alloy 15-15Ti have been used, following [18]. In particular, the density is derived from experimental data presented in [39], and the conductivity is a fitted correlation from [40].

$$\rho_{\text{clad}}(T) = 8138.6 - 0.24855 \cdot 10^{-2}\, T - 1.0239 \cdot 10^{-4}\, T^2 + 4.2893 \cdot 10^{-9}\, T^3 \quad \left[\text{kg m}^{-3}\right]$$
$$\lambda_{\text{clad}}(T) = 7.598 + 2.391 \cdot 10^{-2}\, T - 8.899 \cdot 10^{-6}\, T^2 \quad \left[\text{W m}^{-1}\,\text{K}^{-1}\right]$$

As for the cladding-pellet cap, the conductivity has been taken as the one for helium gas, for simplicity:

$$\lambda_{\text{gap}}(T) = -0.0095\frac{1}{T} + 0.00285\, T^{0.7} + 3.1 \cdot 10^{-6}\, T + 2.9 \cdot 10^{-10}\, T^2 \quad \left[\text{W m}^{-1}\,\text{K}^{-1}\right]$$

Fluid dynamics correlations

Some of the following correlations for common non-dimensional parameters in fluid dynamics are already present in the body of the text, and are included here for reference.

$$\begin{aligned}
\text{Re}(T, v) &= \frac{\rho(T)\, v\, D_h}{\mu(T)} \\
\text{Pr}(T) &= \frac{\mu(T)\, c_p(T)}{\lambda(T)} \\
\text{Pe}(T, v) &= \text{Re}(T, v) \cdot \text{Pr}(T) \\
\text{Nu}(T, v, \text{PDR}) &= 0.047 \left(1 - \text{e}^{-3.8(\text{PDR}-1)}\right) \left(\text{Pe}(T, v)^{0.77} + 250.0\right)
\end{aligned}$$

Appendix B Derivations

Neutron flux distribution in a bare cylindrical core. Peaking factors

The *one-group reactor equation* is obtained by postulating a neutron flux ϕ verifying the diffusion equation (see [33]), where ∇ is the Laplacian operator and B is a real constant:

$$\nabla^2\phi + B^2\phi = 0 \tag{B.1}$$

For the specific case of cylindrical coordinates with coordinates (r, z) (since the system features axial symmetry, no angular dependence is present), the reactor equation reads

$$\frac{1}{r}\frac{\partial}{\partial r}r\frac{\partial\phi}{\partial r} + \frac{\partial^2\phi}{\partial z^2} + B^2\phi = 0 \tag{B.2}$$

This is can be solved in the standard way using separation of variables, i.e. assuming

$$\phi(r, z) = R(r)Z(z) \tag{B.3}$$

and substituting into the reactor equation, two ordinary differential equations are obtained, one for each variable:

$$\frac{d^2R}{dr^2} + \frac{1}{r}\frac{dR}{dr} + B_r^2R = 0 \tag{B.4}$$

$$\frac{d^2Z}{dz^2} + B_z^2Z = 0 \tag{B.5}$$

Where the buckling B^2 verifies

$$B^2 = B_r^2 + B_z^2 \tag{B.6}$$

The equation for $Z(z)$ solves immediately for a linear combination of $sin(z)$ and $cos(z)$; since the solution must be z-symmetric and verify the boundary conditions that $Z(-\tilde{H}/2) = Z(+\tilde{H}/2) = 0$, then since only the first harmonic will be present at steady state it follows that

$$Z(z) = A_z \cos\left(\frac{\pi z}{\tilde{H}}\right) \tag{B.7}$$

On the other hand, the equation for $R(r)$ is a particular case of the well-known *Bessel equations*, which feature as solution linear combinations of the *Bessel functions*. Given, specifically, the boundary conditions and that the solution must be bounded, the solution is the Bessel function of order zero of the first kind, $J_0(Br)$, appropriately scaled:

$$R(r) = A_r J_0\left(\frac{2.405r}{\tilde{R}}\right) \tag{B.8}$$

since $x \simeq 2.405$ is the first root of $J_0(x)$. Therefore, the overall neutron flux is

$$\boldsymbol{\phi(r,z) = R(r)Z(z) = A\,J_0\left(\frac{2.405r}{\tilde{R}}\right)\,\cos\left(\frac{\pi z}{\tilde{H}}\right)} \tag{B.9}$$

Note that from this flux distribution the peaking factors may be obtained. In the specific case of the reflected reactor where $\tilde{R} = 1.5R$ and $\tilde{H} = 1.5H$, as postulated throughout the work, one finds, respectively:

$$\begin{aligned} F_R =& \frac{\phi^{max}}{\bar{\phi}|_{\mathrm{R}}} = \\ =& \frac{A}{\frac{1}{A_{\mathrm{core}}}\int \phi|_R \,\mathrm{d}A} = \frac{A}{\frac{1}{\pi R^2}\int_0^R A J_0\left(\frac{2.405r}{\tilde{R}}\right)\cdot 2\pi r \mathrm{d}r} = \frac{A}{\frac{2A}{R^2}\int_0^R r\, J_0\left(\frac{2.405r}{\tilde{R}}\right)\mathrm{d}r} \simeq \\ \simeq& \frac{A\,R^2}{2A\,R^2\cdot 0.355649} = \mathbf{1.406} \end{aligned}$$

and

$$\begin{aligned} F_Z =& \frac{\phi^{max}}{\bar{\phi}|_{\mathrm{Z}}} = \\ =& \frac{A}{\frac{1}{H_{\mathrm{core}}}\int \phi|_Z \,\mathrm{d}z} = \frac{A}{\frac{1}{\tilde{H}}\int_{-H/2}^{+H/2} A\cos\left(\frac{\pi z}{\tilde{H}}\right)\mathrm{d}z} = \frac{A}{\frac{A}{\tilde{H}}\int_{-H/2}^{+H/2}\cos\left(\frac{\pi z}{\tilde{H}}\right)\mathrm{d}z} \simeq \\ \simeq& \frac{A\,H}{A\,H\cdot 0.826993} = \mathbf{1.209} \end{aligned}$$

Fuel assembly pitch

In Equation (2.50), the pitch has been expressed as follows by substituting the values for the coolant channel area and for the hydraulic diameter:

$$p = \frac{8}{\pi} \frac{\frac{F_R \, \dot{Q}_{nom}}{2 \, N_{rod} \, \rho_{Pb} \, v_{nom} \, c_p \, \Delta T}}{\left(\frac{aK H_{ch}}{2g \, \Delta\rho_{Pb}(\Delta T) \, H_{DC}} {\rho_{Pb}}^{1-b} \, {v_{nat}}^{2-b} \, {\mu_{Pb}}^{b} \right)^{1/1+b}} \tag{B.10}$$

From here, after rearranging and simplifying, one obtains

$$p = \frac{4}{\pi} \frac{F_R \dot{Q}_{nom}}{N_{rod} c_p \Delta T} \left[\frac{2g \Delta\rho H_{DC}}{aK H_{ch} \mu^b \rho^2 {v_{nom}}^3} \right]^{1/1+b} \frac{1}{\left(\dot{Q}_{res} / \dot{Q}_{nom} \right)^{\frac{2-b}{1+b}}} \tag{B.11}$$

At this point one applies that, as per Equations (2.33) and (2.39),

$$H_{ch} \, {v_{nom}}^3 = H_{ch} \left(\frac{v_{nat}}{\dot{Q}_{res} / \dot{Q}_{nom}} \right)^3 = \frac{1}{\left(\dot{Q}_{res} / \dot{Q}_{nom} \right)^3} \mu \, \mathrm{Re}^{1+b} \frac{2g \Delta\rho H_{DC}}{aK\rho^2} \tag{B.12}$$

And that therefore substituting (B.12) into (B.11) simplifies further to, after rearranging:

$$\boldsymbol{p = \frac{4}{\pi} \frac{F_R \, \dot{Q}_{nom}}{N_{rod} \, c_p \, \Delta T} \frac{1}{\mu_{Pb} \, Re_{nat}^{min}} \left(\frac{\dot{Q}_{res}}{\dot{Q}_{nom}} \right)} \tag{B.13}$$

Hexagonal fuel assembly geometry

Both the fuel pins within the fuel assembly, and the fuel assemblies within the core, are organized in a hexagonal grid, as seen e.g. in Figure 2.1a. This implies that only specific values of pins per assembly and assemblies are possible, namely those that correspond to full hexagonal *rings* on the layout.

In particular, the number of pins in an assembly must be

$$N_{\text{pins, assembly}} = 3 \, n \, (n+1) + 1 \tag{B.14}$$

Where n is the number of *rings*. The range of possible pins per assembly has been set, considering the range seen in actual fast reactor fuel assemblies, to be between $N_{\text{pins, assembly}} = 37$ $(n = 3)$ and $N_{\text{pins, assembly}} = 397$ $(n = 11)$.

On the other hand, the number of assemblies is also constrained by a similar expression, but with two differences: the central assembly is removed, in order to achieve a flatter neutron distribution, and furthermore the 6 "corner" assemblies are also avoided on the last ring (except for the case of cores with only 1 or 2 rings of assemblies); this improves the neutron economy (it can be thought as making the core more "cylindrical"). Then, the corresponding expression for the number of assemblies is

$$M_{\text{assemblies}} = 3\,m\,(m+1) - 6 \tag{B.15}$$

with m being here the number of rings of assemblies in the core. Therefore, the minimum number of rods in the core in total corresponds to 6 assemblies of 37 pins each, i.e.

$$N_{rod} = M_{\text{assemblies}} \cdot N_{\text{pins, assembly}} = 6 \cdot 37 = 222 \tag{B.16}$$